Physics – Uspekhi **55** (9) 845 – 875 (2012)

REVIEWS OF TOPICAL PROBLEMS

PACS numbers: 05.45.Tp, 05.45.Xt, 07.05.Mh, 87.19.L –, 95.75.Wx

Wavelet analysis in neurodynamics

A N Pavlov, A E Hramov, A A Koronovskii,
E Yu Sitnikova, V A Makarov, A A Ovchinnikov

DOI: 10.3367/UFNe.0182.201209a.0905

Contents

Abstract. Results obtained using continuous and discrete wavelet transforms as applied to problems in neurodynamics are reviewed, with the emphasis on the potential of wavelet analysis for decoding signal information from neural systems and networks. The following areas of application are considered: (1) the microscopic dynamics of single cells and intracellular processes, (2) sensory data processing, (3) the group dynamics of neuronal ensembles, and (4) the macrodynamics of rhythmical brain activity (using multichannel EEG recordings). The detection and classification of various oscillatory patterns of brain electrical activity and the development of continuous wavelet-based brain activity monitoring systems are also discussed as possibilities.

A N Pavlov, A A Koronovskii, A A Ovchinnikov
N G Chernyshevsky Saratov State University,
ul. Astrakhanskaya 83, 410012 Saratov, Russian Federation
Tel. +7 (8452) 21 07 20, +7 (8452) 51 42 94. Fax +7 (8452) 52 38 64
E-mail: pavlov.lesha@gmail.com, alkor@nonlin.sgu.ru,
a.a.ovchinnikov@gmail.com
A E Hramov N G Chernyshevsky Saratov State University,
ul. Astrakhanskaya 83, 410012 Saratov, Russian Federation
Tel. +7 (8452) 51 42 94. Fax +7 (8452) 52 38 64
E-mail: hramovae@gmail.com
Yu A Gagarin Saratov State Technical University,
ul. Politekhnicheskaya 77, 410054 Saratov, Russian Federation
E Yu Sitnikova Institute of Higher Nervous Activity
and Neurophysiology, Russian Academy of Sciences,
ul. Butlerova 5A, 117485 Moscow, Russian Federation
E-mail: eu.sitnikova@gmail.com
V A Makarov Universidad Complutense de Madrid, F.CC. Matemáticas,
Avda. Complutense s/n, 28040 Madrid, Spain
E-mail: vmakarov@mat.ucm.es

Received 6 October 2011, revised 18 March 2012
Uspekhi Fizicheskikh Nauk **182** (9) 905 – 939 (2012)
DOI: 10.3367/UFNr.0182.201209a.0905
Translated by Yu V Morozov; edited by A Radzig

> *Wavelets are a relatively new discovery in applied mathematics. The name itself emerged some ten years ago... . There has been an explosion of interest in them over the last decade... . Because of their interdisciplinary origin, wavelets appeal to scientists and engineers of many different backgrounds... .*
> Ingrid Daubechies (from the Introduction to *Ten Lectures on Wavelets* [17]

1. Introduction

Modern neurodynamics constitutes an extensive interdisciplinary field of natural sciences, which is closely related to neurophysiology and wherein basic knowledge about the principles and mechanisms of the functioning of the nervous system comes from the joint experience of chemists, biologists, physicists, mathematicians, and specialists in nonlinear theory of oscillations and waves [1–3]. Recent progress in understanding molecular and ionic mechanisms underlying the activity of individual neurons [4] provided a basis for further investigations into such essentially physical problems

as exploration of the functional properties and principles of information coding, its representation and processing in the sensory data in the central nervous system (CNS). The perception and processing of external information are the main functions of the CNS. Visual, acoustic, tactile, and gustatory stimuli are transformed by respective receptors into a sequence of electrical pulses. These nervous pulses propagate through afferent nerve fibers from receptor cells to 'primarily feeling' neurons that carry out the primary processing of sensory information [5–8]. This sensory information is then passed through a few relay stations (brain stem and thalamic nuclei) that transform and convolve the information code, before it reaches the cerebral cortex where an image of the external world is formed [9, 10]. At each subsequent stage of information transfer, the relevant processes are increasingly more difficult to study. The question of how the totality of nervous impulses (action potentials or spikes) generated by single neurons reflect the all complexity and diversity of the external world remains one of the biggest challenges for the natural sciences.

Recent years have witnessed considerable progress in the development of experimental methods for studying the production and propagation of signals at different stages — from receptor cells to the cerebral cortex. Noninvasive methods of recording and analyzing the overall brain electrical activity, such as electroencephalography (EEG) with electrodes arranged on the skin of the head, are also still in use. EEG is frequently utilized to study brain functions in humans and other animals [11, 12]. There are also invasive methods employing implanted electrodes, which provide more detailed information on the electrical activity of small neuron populations in the cortex and subcortical structures. Magnetic encephalography (MEG) is finding increasingly wider application in the last few years due to the higher quality of signals reflecting brain activity [13].

The technical progress in experimental studies is paralleled by the lack of concordance with the mathematical apparatus applied in neurophysiological research. The overwhelming majority of the experimental work in this field makes use of very few statistical methods for treating the data obtained, e.g., calculation of the mean spike frequency, construction of various correlation characteristics and distribution functions, etc. It should be emphasized, without lessening the importance of statistical methods in biology, that not infrequently they provide only limited information about the complicated phenomena encoded in experimental data. This fact is illustrated by the example of the study of the response of a sensory neuron to periodic stimulation. If all neurons similarly reacted to the same external action (e.g., a short electrical pulse), periodic stimulation by a series of impulses would induce a periodic sequence of spikes (e.g., 2 or 3 spikes per stimulus). However, experimentalists not infrequently encounter time-varying neuron responses due, in particular, to the adaptation to external factors, which is attributable to both the intrinsic characteristics of a single cell and the dynamics of the neural network as a whole [14, 15]. As is also known, the neuron can even stop responding to the next stimulus from a certain moment. Figure 1 illustrates the adaptive response of a neuron of the trigeminal complex to periodic stimulation. Maximum neuron activity (27 spikes/s) is observed at the onset of stimulation; it falls to average 10 spikes/s within a few seconds and varies thereafter, undergoing a slow negative drift. On the one hand, such a behavior of the living system makes it extremely difficult to

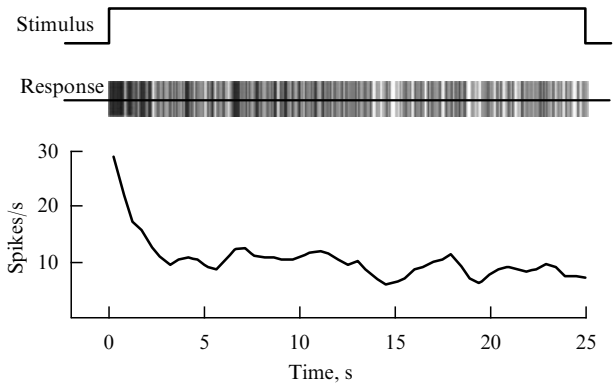

Figure 1. An example of the adaptation of neuron firing activity in the rat trigeminal complex perceiving tactile information from vibrissae in response to long periodic mechanical stimulation of one of the whiskers by directed short (50 ms) air puffs. From top to bottom: the beginning and end of stimulation by the sequence of periodic impulses; neuron-generated spike train, and dynamics of the mean spike frequency (averaging over a sliding window of 500 ms duration).

single out characteristic modes of neural activity that could be associated with the peculiar properties of a given stimulus. On the other hand, it is clear that the study of sensory data processing should not be restricted to simple statistical characteristics; additional specific methods more suitable for decoding information contained in the processes with time-varying features are needed. Wavelet analysis [16–19] is one such method: even first attempts of its application in neurophysiological research [20–24] has demonstrated the high potential of wavelets for studying the dynamics of neural systems.

Wavelet terminology was developed in the 1980s [16, 25]. This mathematical apparatus was initially proposed as an alternative to classical spectral analysis based on the Fourier transform. The advent of the wavelet theory is considered to be a very important event in mathematics in the past decades; indeed, it appears to be the sole new mathematical concept that was immediately recognized as a tool for applied research in practically all natural sciences (first and foremost, in physics) and many technical fields [26–34]. To recall, the appearance of the wavelet theory itself was not unexpected, since it was dictated by the real needs of experimental investigations. Modern wavelet analysis is essentially a combination of pre-existing ideas and methods. For example, fast wavelet transform algorithms are based on the subband coding ideology known from radioengineering [35]. Some ideas were borrowed from physics (coherent states [36], etc.) and mathematics (studies on Caldéron–Zygmund integral operators [37]).

Today, wavelets are widely used in work involving the analysis and synthesis of various signals, image processing and recognition, the compaction of large volumes of information, digital filtration, studying intense turbulence, and the solution of certain differential equations. This list can certainly be extended [38–47]. In particular, there are numerous examples of the application of wavelet analysis in modern physics, including active and passive radar, radiometry, radar technical security devices, communication systems, cosmology, acoustics, fluid dynamics, turbulence structure, solid-state physics, processes of multiparticle production, analysis and diagnostics of structure formation, chaotic synchronization, geophysics, seismology and so forth [26, 32–34, 36, 48–60]. The new theory aroused great interest

from the very beginning. According to known estimates [28], starting in the 1990s the number of publications based on the study of physical phenomena with the use of wavelets is growing continuously. The number of references to Internet sources containing the term 'wavelet' amounts to several million. In the natural sciences, this mathematical apparatus is most extensively applied to characterize temporally nonstationary or spatially inhomogeneous complex nonlinear processes. It is for this reason that wavelet analysis is of strong interest for structural studies of signals from living systems, most classical digital data processing methods being applicable only to processes with time (or space)-constant parameters. Wavelet analysis long ago became a standard tool for studying complex processes, and the success achieved with its help gives reason for optimism. Nevertheless, its application in biology and medicine is still in its infancy; hence, the necessity and importance of reviewing such applications in neurodynamics for the systematization of various interdisciplinary approaches and the results of relevant research.

Details of the mathematical apparatus of wavelet analysis have been described in two comprehensive reviews [32, 33]. The present review is focused on new possibilities provided by the wavelet analysis for decoding information contained in the signals from individual neurons and neural networks. The review layout is as follows. Section 3 is devoted to wavelet application for the analysis of microscopic dynamics at the level of single cells or intracellular processes. The problems of analysis of information contained in the signals of electrical activity of small neural assemblies are discussed in Section 4. The use of wavelets for the analysis of electroencephalograms (EEGs) is described in Section 5. This material is largely based on the results of research carried out by the authors in recent years in close collaboration with practising neurophysiologists. By and large the wavelet-based methods discussed in the review and their physiological interpretation are good examples of the application in neurodynamics and neurophysiology of modern analytic and diagnostic techniques developed in physics and nonlinear dynamics. Moreover, the results obtained with the help of wavelet analysis are frequently the first steps to understanding the nature of the phenomena under investigation. Extensive research in this field can promote interdisciplinary cooperation and further cross-fertilization of physics, radiophysics, applied mathematics, and neurophysiology.

It should be noted that applications of the approaches to the analysis of neural systems considered in the framework of this review are not restricted to neurodynamics and neurophysiology. Suffice it to say that distinguishing meaningful signals from background noise and the modulation, detection, and diagnostics of temporal and spatial–temporal structures in nonlinear systems are of paramount importance for modern radiophysics and nonlinear dynamics. It is these and similar problems on which the present review is actually focused. Indeed, the methods used to detect and classify neuronal spikes are suitable for the recognition of a group of objects and the determination of distances to them in radar. Approaches to the recognition of characteristic EEG oscillatory patterns are equally applicable to the discrimination of voice messages from intense noise, the diagnostics of spatial structures in plasma-based systems, etc.

Wavelet analysis is a popular research tool increasingly in demand among specialists interested in both fundamental and applied problems. We are earnestly convinced that a wider application of this instrument would significantly broaden the scope of many theoretical and especially experimental research avenues in various fields of physics and related sciences.

2. General information about wavelets

In analogy with the Fourier transform, the wavelet transform of a signal $x(t)$ consists in its expansion on a certain basis. The difference lies in the choice of a 'soliton-like' function $\psi(t)$ for the basis function having some characteristic properties and well-localized in time and frequency domains; the basis is formed by transition to another scale of $\psi(t)$ and its shifts along the time axis. The employment of localized functions makes possible the analysis of processes whose characteristics vary with time; also, this provides a means for the two-dimensional scanning of the signal $x(t)$, at which both the time and the frequency are regarded as independent variables [32].

Wavelet analysis, unlike the classical spectral one, permits significantly diversifying the choice of the basis on which the signal is expanded. The harmonic functions applied in the framework of the Fourier transform are specified on the interval $t \in (-\infty, \infty)$ and do not permit effectively investigating local changes in the signal structure.[1] Calculation of the power spectrum density of signal $x(t)$ makes it possible to determine the frequency composition of the process being considered and to elucidate characteristic oscillation rhythms. It allows the presence of oscillations at a definite frequency to be demonstrated but does not show when these oscillations occurred (during the entire signal recording time or within a shorter interval). Infinitely oscillating functions cannot be used for the purpose of localized spectral analysis [31]. What, then, are basis functions (wavelets)? If the $\psi(t)$ function is to be regarded as a wavelet, it should have a number of characteristic properties, i.e., be localized in time and frequency, zero mean, and finite energy [32, 33].

There are discrete and continuous wavelet transforms that can be regarded as different methods for the analysis of signal structure. The continuous wavelet transform (CWT) utilizes functions ('mother' wavelets) infinitely differentiable and usually having the analytical form.[2] Due to this, the functions exponentially decrease at infinity and the basis constructed using such wavelets is not strictly orthonormalized. This feature means that the CWT is redundant and the values of wavelet transform coefficients are strongly correlated. However, the redundancy may prove to be a useful property allowing one to obtain a more demonstrative and clearer interpretation of the results of the signal structure analysis in the form of 'skeleton' or 'ridge' patterns and surface level lines of wavelet transform coefficients [31]. Information that can be derived from a continuous wavelet transform (e.g., about changes in the characteristic frequencies of rhythmic processes and their interaction) is easier to analyze, such a presentation being reminiscent of the radiophysical one [63]. When complex functions $\psi(t)$ are applied, the CWT permits studying the dynamics of such character-

[1] It should be noted that there is a windowed Fourier transform which also permits processing of nonstationary signals. Monograph [29] reviews advantages and disadvantages of this transform and illustrates the possibility of a passage from the windowed Fourier transform to wavelets.
[2] We note that 'mother' wavelets can also be constructed on the basis of tabulated time-series fragments [61, 62].

istics as instantaneous amplitudes, frequencies, and phases of rhythmic processes, which are identified in the structure of the signal being analyzed. When phases are the study subject, it is possible to introduce into consideration families of time signal phases corresponding to various independent spectral components of the signal [48, 64–66]. Such possibilities make CWT a highly attractive tool for the solution to many problems.

Discrete wavelet transform (DWT) is essentially different from CWT. It can utilize nonorthogonal basis functions (frames) [17]. However, an orthonormalized (or almost orthonormalized) basis is usually considered, which makes possible a more accurate representation of the signal and significantly simplifies its reconstruction from a set of wavelet coefficients. Unlike CWT wavelets, DWT wavelets do not have the analytical recording form (with the exception of the Haar function [18]). They are given in the form of a table of numerical coefficients obtained by the solution of certain equations. In practice, the concrete form of $\psi(t)$ functions in the framework of DWT is not considered in the explicit form — only sets of numbers are written out that are used to specify any given wavelet. This implies a series of elementary operations with matrices, which makes possible realization of fast DWT calculation algorithms. The basis is constructed using the iteration algorithm, making allowance for a change in the scale and a shift of the unique function. The detailed description of essential differences between the DWT and CWT procedures can be found in book [28]. This section is only confined to the data on the two aforementioned transforms, which will be needed in the following.

2.1 Continuous wavelet transform

The characteristic signs formulated above define a large class of real-valued and complex wavelets involved in solving a variety of problems. Specifically, the Morlet wavelet [16] is most popular among complex functions used in the local spectral analysis of processes with time-varying characteristics, being well localized in time and frequency:

$$\psi(t) = \frac{1}{\pi^{1/4}}\left[\exp\left(\mathrm{i}2\pi f_0 t\right) - \exp\left(-\frac{(2\pi f_0)^2}{2}\right)\right]\exp\left(-\frac{t^2}{2}\right), \tag{1}$$

where f_0 is the parameter called central frequency, and $\mathrm{i} = \sqrt{-1}$. The second term in brackets performs a correction for a wavelet transform of signals with the nonzero mean. It can be neglected in the case of $f_0 > 0$.

The chosen 'mother' wavelet $\psi(t)$ is used to form the basis. Function $\psi(t)$ is localized in time; in order to analyze different portions of the $x(t)$ signal with the help of this function, a shift along the t-axis is needed to enable displacement into these portions. On the other hand, the localized analysis of the signal structure in a wide scale (frequency) range implies a transition to another scale. As a result, function $\psi(t)$ provides the basis for the construction of the two-parameter wavelet family

$$\psi_{a,b}(t) = \frac{1}{\sqrt{a}}\,\psi\left(\frac{t-b}{a}\right), \tag{2}$$

where parameter $a \in \mathbb{R}$, $a > 0$, called the scale of the wavelet transform, is the scale factor that determines the compression or extension of the function; $b \in \mathbb{R}$ is the shift parameter, with the help of which the wavelet moves along the signal $x(t)$ being analyzed, and $\mathbb{R}$ is the real number space. Factor $1/\sqrt{a}$ serves to normalize the energy of each $\psi_{a,b}(t)$ function, so that its L^2 norm is constant: $||\psi_{a,b}(t)||_{\mathrm{L}^2} = ||\psi(t)||_{\mathrm{L}^2} < \infty$.

Thus, the continuous wavelet transform of signal $x(t)$ defined in the time interval $-\infty < t < \infty$ has the following form

$$W(a,b) = \frac{1}{\sqrt{a}}\int_{-\infty}^{\infty} x(t)\,\psi^*\left(\frac{t-b}{a}\right)\mathrm{d}t = \int_{-\infty}^{\infty} x(t)\,\psi^*_{a,b}(t)\,\mathrm{d}t\,, \tag{3}$$

where the superscript '$*$' denotes a complex conjugation. If $W(a,b) \in \mathbb{R}$, the result of transformation (3) can be regarded as a surface in the three-dimensional space.[3] There are different variants of visualization of this surface for the pictorial representation of peculiar features of the signal being analyzed. One is consideration of its projection onto the (a,b) plane and depicting the values of wavelet transform coefficients in different colors (as on geographic maps). Such an approach makes it possible to see how signal properties vary with time on different time scales.[4]

The so-called wavelet transform ridges are usually constructed to identify instantaneous characteristics of rhythmic processes (amplitudes, frequencies, phases) [28]. The ridges are constructed for the signal energy density surface $E(a,b) = |W(a,b)|^2$; they actually represent lines of local maxima of such a surface (identified when fixing time moment $b = t_*$ and considering local energy spectra). Not infrequently, it is more convenient to consider surface $E(f,b)$ instead of $E(a,b)$, i.e., to pass to the frequency representation of the energy spectrum. However, it should be taken into consideration that the relationship between timescale a and frequency f depends on both the type of the wavelet function chosen and its parameters. Specifically, the relation between the scales of the wavelet transform and the frequencies of the Fourier spectrum for wavelet (1) takes the form

$$f = \frac{f_0}{2a} + \frac{\sqrt{2 + 4(\pi f_0)^2}}{4\pi a}\,.$$

This is a very convenient and an easy-to-grasp method for the analysis of nonstationary multifrequency dynamics, making it possible to trace the time evolution of each oscillation rhythm of interest to the researcher. Each point at the ridge being associated with the local energy spectrum, the finding of instantaneous frequencies of oscillation processes ensures at the same time the determination of their instantaneous amplitudes and the instantaneous phase (if a complex wavelet is utilized):

$$\varphi_a(b) = \arg W(a,b)\,. \tag{4}$$

This variant of analysis will be applied in studies of neural system dynamics at the microscopic level, and nonstationary EEG dynamics.

2.2 Multiscale wavelet analysis

It was assumed in the discussion of the continuous wavelet transform in Section 2.1 that the $x(t)$ signal is expanded in the basis constructed from one soliton-like function $\psi(t)$ or

[3] It is easy to show that for a large class of $x(t)$ signals (actually, for any physical processes), $W(a,b) \in \mathrm{C}(\mathbb{R}\times\mathbb{R})$, where C is the continuous function space.

[4] Note that the range of frequencies being studied is bound by the length L of the time series ($f_{\min} \sim 1/L$) from below, and by discretization frequency f_{s} ($f_{\max} = f_{\mathrm{s}}/2$) from above.

'mother' wavelet. The multiple-scale analysis exploiting the discrete wavelet transform is based on a different ideology. The orthonormalized wavelet bases are utilized in this method in order to describe mathematically the 'information gain' needed to pass from a rough approximation to a more accurate one [18, 19]. This concept emerged for the first time in the solution to applied problems of image analysis.

In the framework of the multiple-scale analysis, scaling function $\varphi(t)$, sometimes called the 'paternal' wavelet, is introduced into the consideration. The following equality is fulfilled for the scaling function:

$$\int_{-\infty}^{\infty} \varphi(t)\,\mathrm{d}t = 1\,, \tag{5}$$

i.e., its mean value is not zero, as in the case of 'mother' wavelet $\psi(t)$.

Let us introduce the following notation in analogy with formula (2):

$$\varphi_{j,k}(t) = \frac{1}{2^{j/2}}\,\varphi(2^j t - k)\,. \tag{6}$$

At different values of the scale transform coefficient and displacement, corresponding to parameters j and k, the approximation coefficients can be calculated as follows:

$$s_{j,k} = \int_{-\infty}^{\infty} x(t)\,\varphi_{j,k}(t)\,\mathrm{d}t\,. \tag{7}$$

For the chosen resolution level, the coefficients thus obtained are referred to as discrete approximations of the signal on scale j. Summation of the scaling functions and the respective coefficients yields the so-called continuous approximation of signal $x(t)$ on a given scale or resolution level j [18]:

$$x_j(t) = \sum_{k=-\infty}^{\infty} s_{j,k}\,\varphi_{j,k}(t)\,. \tag{8}$$

On small scales (large j), this continuous approximation approaches the signal $x(t)$ being analyzed. The ideology of this continuous approximation permits describing the 'trend' of the process of interest on the chosen observation scale; thereafter, a detailed analysis of fluctuations with respect to this trend can be undertaken with the help of wavelets.

Any function $x(t) \in \mathrm{L}^2(\mathbb{R})$ can be represented at a certain arbitrary resolution level j_n as the series

$$\begin{aligned} x(t) &= \sum_k s_{j_\mathrm{n},k}\varphi_{j_\mathrm{n},k}(t) + \sum_{j \geqslant j_\mathrm{n}} \sum_k d_{j,k}\,\psi_{j,k}(t)\,, \\ \psi_{j,k}(t) &= 2^{j/2}\psi(2^j t - k)\,, \end{aligned} \tag{9}$$

where $\psi_{j,k}$ are the scaled and displaced versions of the mother wavelet. The expansion coefficients $d_{j,k}$ are defined as

$$d_{j,k} = \int_{-\infty}^{\infty} x(t)\,\psi_{j,k}(t)\,\mathrm{d}t\,. \tag{10}$$

Using approximation (8), it is possible to write out the expression for the chosen scale (resolution level) j_n:

$$x(t) = x_{j_\mathrm{n}}(t) + \sum_{j \geqslant j_\mathrm{n}} \mu_j(t)\,, \tag{11}$$

where the function

$$\mu_j(t) = \sum_k d_{j,k}\,\psi_{j,k}(t) \tag{12}$$

characterizes the detailed structure of the signal on the resolution level j. Using formula (11), it is possible to write the recurrent expression

$$x_{j+1}(t) = x_j(t) + \mu_j(t)\,; \tag{13}$$

in other words, supplementation of the approximation on an arbitrary scale j by detalization of signal $\mu_j(t)$, describing fluctuations with respect to the trend being approximated, yields the approximation on the next, more detailed resolution level $j+1$. The reader is referred to review [33] for an extended description of the multiple-scale analysis (also called multiscale analysis).

In practice, the value of the scale transform coefficient 2^j is limited on small and large scales. It is clear that the signal structure cannot be analyzed on scales smaller than a single discretization interval Δt (the scale of a resolved structure) or scales larger than signal duration $N\Delta t$ that is, practically speaking, finite (and can be comparatively short). This accounts for the limitation on the variation of j that determines the confidence level of the conclusions about the structure of the process being analyzed on one scale or another (frequencies).

3. Dynamics of individual neurons

After the brief introduction to the theory of wavelet analysis, we shall consider problems, in the solution of which wavelets help to gain new information about the dynamics of neural systems. These problems can be categorized into a few groups, depending on the mathematical apparatus applied (DWT or CWT). However, the choice of the transform type is often unessential. Different mathematical approaches may be complementary and give a more comprehensive idea about the functioning of the study objects. For this reason, we choose another variant, i.e., to differentiate between problems depending on the study object (single cells, large neural assemblies, etc.).

3.1 Analysis of intracellular dynamics

Let us start by turning to the microscopic level, i.e., to intracellular processes, and the application of wavelet analysis. Neural activity is known to be underlain by a variety of biochemical processes proceeding on different time scales at the level of cell membrane and cytoplasm. Information on the relationship between these processes may provide a deeper insight into the mechanisms regulating intracellular dynamics. Traditional experimental techniques (intracellular recording of membrane potentials, fluorescence microscopy, etc.) permit studying various processes in a single neuron, but many of them are highly invasive. As a consequence, some traditional methods may affect intracellular processes and even cause damage to a cell.

References [67–69] report on dynamic studies of intracellular processes by interference microscopy based on the measurement of the optical path difference between a laser beam passed through a given object and then reflected from a mirror under the object and a beam reflected from the reference mirror [70]. The measured quantity is normalized

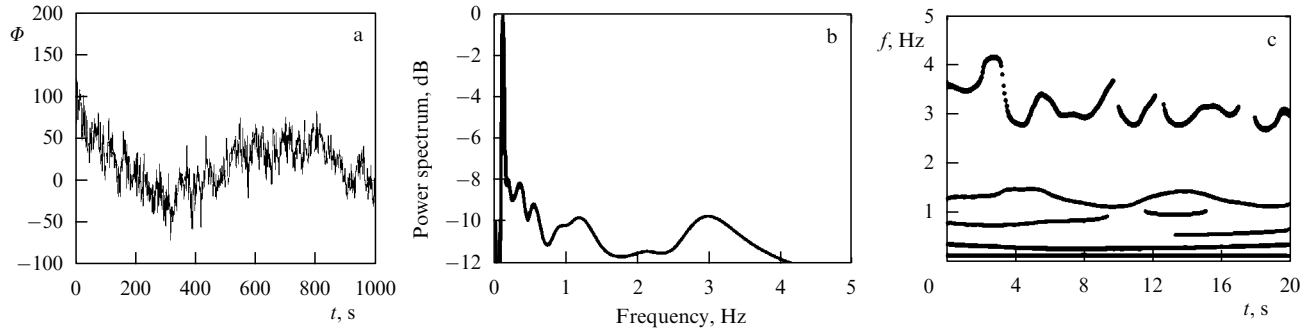

Figure 2. Time dependence of the phase height at one of the points (a) and results of its spectral analysis based on a continuous wavelet transform (b, c).

to the light wavelength in order to obtain the so-called 'phase height' of the object at a concrete point:

$$\Phi = \frac{\phi_0 - \phi_{\text{obj}}}{2\pi}\,\frac{\lambda}{2} - \Phi_0\,. \tag{14}$$

Here, ϕ_0 is the initial phase, ϕ_{obj} is the phase shift after passage through the object, λ is the laser wavelength, and Φ_0 is the constant phase shift determined by the choice of the zero phase reference point. For inhomogeneous objects characterized by varying refractive index, the phase height equals

$$\Phi(x,y) = \int_0^Z \bigl(n_{\text{obj}}(x,y,z) - n_{\text{s}}\bigr)\,\mathrm{d}z - \Phi_0\,, \tag{15}$$

where n_{s} is the constant value of the refraction index in physiological saline, and $n_{\text{obj}}(x,y,z)$ is the refraction index at a point on the cell having coordinates x, y at distance z from the substrate. The integration limit Z is chosen above the topmost point of the object. Measurements of $\Phi(x,y)$ by scanning the cell bring forth its phase image or phase height relief [70].

Various intracellular processes, e.g., organelle motion, tend to change the phase height. A typical signal recorded in the framework of the approach under consideration is shown in Fig. 2a. A few characteristic frequencies can be distinguished in the vicinity of 0.1, 0.3, 1.0, and 3.0 Hz in the signal power spectrum (Fig. 2b). The respective rhythms are caused by a number of intracellular processes, such as protein movements, fluctuations of the transmembrane potential, and subthreshold changes of the membrane potential. Various processes, having different time characteristics, interinfluence one another.

Potential effects of their interaction were estimated by identifying instantaneous frequencies and amplitudes of oscillation processes based on the continuous wavelet transform (3) with the Morlet basis function (1). Figure 2c illustrates the typical behavior of instantaneous frequencies (distinguished by the ridge construction method) at which oscillation rhythms in the range from 0.1 to 0.3 Hz remain almost constant throughout the observation period, whereas instantaneous rhythm frequencies in the range of 1 and 3 Hz undergo slow oscillations [67]. This means that high-frequency fluctuations of the cell phase height are modulated with processes proceeding on longer time scales.[5]

[5] We note that modulation of oscillations is well known from biological system dynamics. It is exemplified by modulation of heartbeats under the effect of respiratory rhythm manifested as an increase in the pulse rate during inhalation and its decrease during exhalation.

The presence of modulation effect means that amplitude A_0 and/or frequency ω_0 of the fast oscillatory process varies in time with a frequency set by the slower process $s(t)$. In the case of amplitude modulation (AM), the following amplitude change may be detected:

$$A(t) = A_0 + \Delta A s(t)\,, \tag{16}$$

where ΔA is the amplitude deviation. The single-tone modulated signal

$$x(t) = A(t)\cos(\omega_0 t + \varphi_0) = A_0\bigl(1 + m_{\text{a}} s(t)\bigr)\cos(\omega_0 t + \varphi_0) \tag{17}$$

contains parameter $m_{\text{a}} = \Delta A/A_0$, called the amplitude modulation coefficient (index).

In the case of frequency modulation (FM), the instantaneous frequency varies according to the law

$$\omega(t) = \omega_0 + \Delta\omega s(t)\,, \tag{18}$$

where parameter $\Delta\omega$ is a deviation (maximum deflection) in the carrier oscillation frequency. An MF signal can be written out as

$$\begin{aligned} x(t) &= A_0\cos\Psi(t) = A_0\cos\left(\int_0^t \omega(t)\,\mathrm{d}t + \varphi_0\right) \\ &= A_0\cos\left(\omega_0 t + \Delta\omega\int_0^t s(t)\,\mathrm{d}t + \varphi_0\right). \end{aligned} \tag{19}$$

In the case of a single-tone FM signal, one has $s(t) = \cos(\Omega t + \Phi_0)$, and consequently

$$x(t) = A_0\cos\bigl[\omega_0 t + \varphi_0 + m_{\text{f}}\sin(\Omega t + \Phi_0)\bigr]\,. \tag{20}$$

Parameter $m_{\text{f}} = \Delta\omega/\Omega$, called the frequency modulation index, characterizes phase deviation of the FM signal. The above formulas become even more complicated for multitone oscillations and under conditions of nonstationary dynamics of objects of an animated nature, when quantities in the expressions for AM and FM indices are variables.

The authors of Refs [67, 71] proposed considering, for the quantitative description of nonstationary multitonal modulation effects, distinguished time dependences of instantaneous frequencies (or amplitudes) of modulated rhythmic processes as the original signals for one more (secondary) wavelet transform allowing a detailed analysis of their structure. Continuous wavelet transform coefficients are calculated, the energy density surface constructed, its ridges deter-

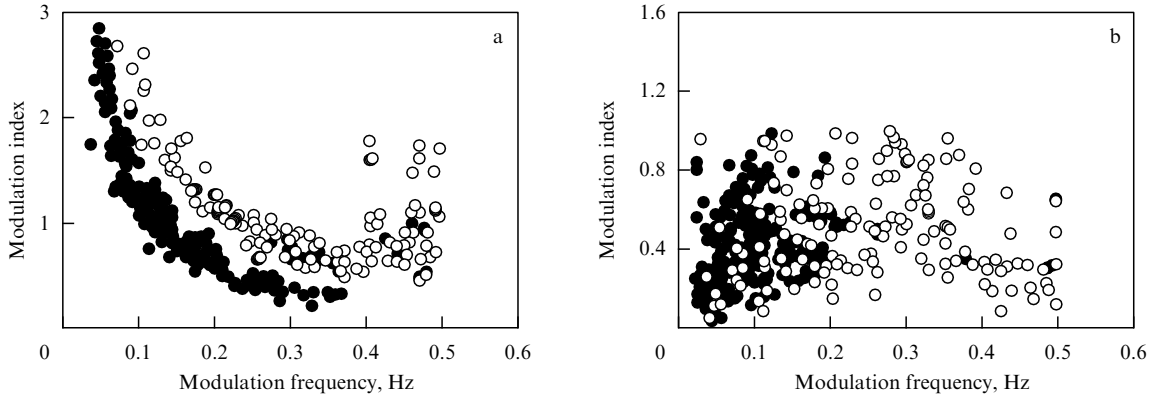

Figure 3. Distribution of the oscillation rhythm modulation indices at 1 Hz (●) and 2–4 Hz (○) for frequency (a) and amplitude (b) modulations.

mined, and the global energy spectrum computed as before. Because signals extracted after a single application of transform (3) can be continuous wavelet transformed, this method is referred to as double wavelet analysis [67, 71, 72]. A similar idea was forwarded independently for the analysis of biological processes in Ref. [73], where the term secondary wavelet transform was adopted. The double wavelet transform method permitted obtaining the time dependences of amplitude and frequency deviations, as well as modulation indices that, in general, could vary in time; also, it was employed to calculate local modulation spectra [74].

Analysis of phase height dynamics allowed slow modulation of the high-frequency oscillation amplitude to be detected along with FM, as illustrated in Fig. 2c. Over 200 experimental records were treated to gather statistical information about peculiarities of AM and FM effects in the dynamics of intracellular processes [67]. The double wavelet analysis was used to estimate the modulation frequency and index. It was revealed that rhythmic components in the vicinity of 1 Hz and 3 Hz are modulated with different processes; namely, the main contribution to modulation of the 1 Hz and 3 Hz rhythms comes from processes with a frequency of 0.1 Hz and higher frequencies, respectively. Figure 3 illustrates the distribution of the oscillation rhythm modulation indices for AM and FM cases. The presence of interaction between slow and fast processes in cell dynamics in the form of modulation of oscillations was for the first time demonstrated in Ref. [67] by the double wavelet transform method; the authors postulated a putative explanation of physiological mechanisms behind the observed effects. The approach being considered may provide a deeper insight into neuron functions and peculiarities of intracellular dynamics, both under the normal conditions of cell functioning and under the action of various external factors. This permits introducing into consideration the quantitative criteria characterizing the influence of certain intracellular processes on others and diagnose changes of this influence under the effect of external factors (see, for instance, Refs [68, 69]).

3.2 Analysis of information coding processes

Decoding information transmitted by neurons has given rise to great interest in modern neurodynamics. Many unanswered questions concerning the principles of coding various stimuli arise, even at the stages of primary treatment of sensory information. Wavelets provide an efficacious tool for gaining insight into the information content of recorded neural signals.

Let us consider this issue in more detail with an example of processing tactile information in rats [75]. These animals receive main sensory information about the external world by actively moving their whiskers or vibrissae (from Latin *vibrare*, to vibrate). The vibrissae constitute a component of the highly organized specialized sensory system conveying information to the upper parts of the brain via the trigeminal complex [76]. Each vibrissa has a specific set of features such as length and location (Fig. 4a). The four longest vibrissae (straddlers) are denoted by letters α, β, γ, and δ. The remaining ones arrayed in five rows on the upper lip are labelled A, B, C, D, and E. The vibrissae within each row are numbered. The length of vibrissae decreases from 30–50 mm to 4–5 mm near the nose to ensure simultaneous contact of their tips with touchable objects and to cover a broad range of space–time frequencies needed for an accurate and efficacious perception of the outside world with the help of this sense organ.

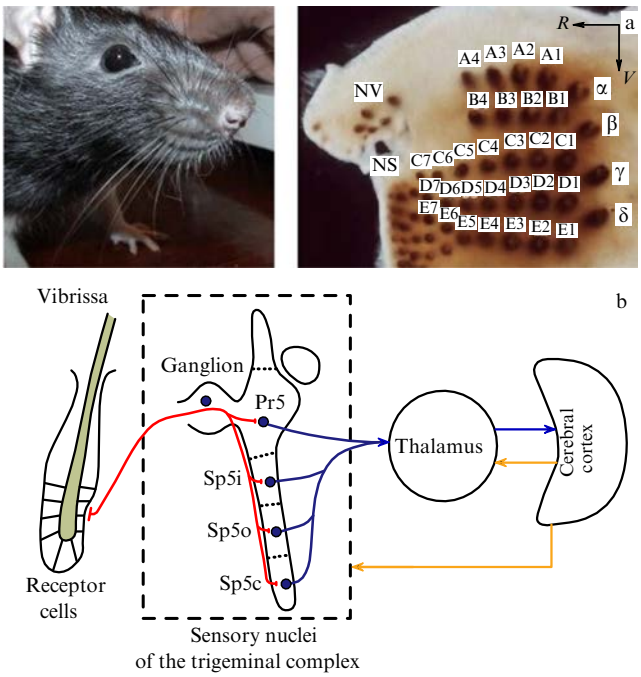

Figure 4. (a) Arrangement of vibrissae. (b) Schematic of the main stages of the sensory information passage from vibrissal mechanoreceptors to the upper brain regions through the trigeminal complex.

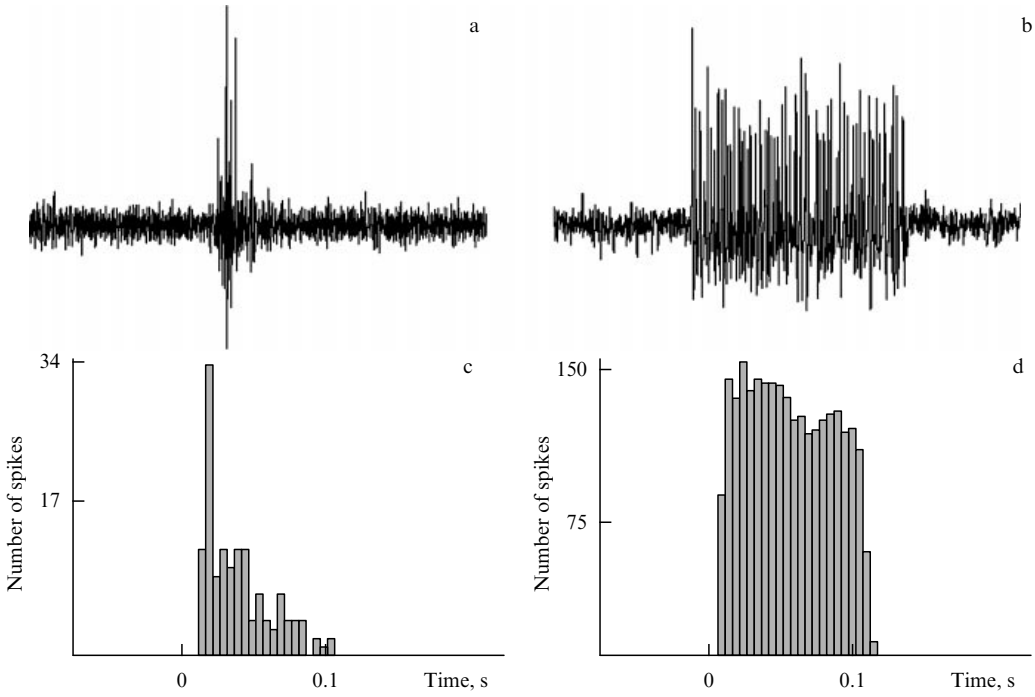

Figure 5. Two characteristic responses of neurons of the trigeminal principal sensory nucleus (Pr5) to mechanical stimulation of a vibrissa. An example of recording the extracellular potential of neurons exhibiting reactions of two types, phasic (a) and tonic (b), in response to stimulation of a single whisker. (c, d) The corresponding cumulative post-stimulus histograms characterizing time interval distribution between the moments of stimulation onset and generation of neural response impulses (the result of averaging over a train of five identical stimuli).

Signals from receptor cells located in vibrissal follicles (Fig. 4b) first arrive at the nuclear complex of the trigeminal nerve [77] composed of the principal sensory (Pr5), oral (Sp5o), interpolar (Sp5i), and caudal (Sp5c) nuclei. This nuclear complex performs primary processing of input sensory information [76, 78]. The majority of the neurons in the Pr5 and Sp5i nuclei transmit sensory information to the thalamus, which sends signals to the cerebral cortex, where tactile images are formed. Neither the Sp5o nor Sp5c nucleus has functionally significant projection paths to the thalamus. All four nuclei interact via the internuclear neural network [79]. When animals palpate objects with their vibrissae, vibrations of the latter trigger spike generation by the cells; the spikes serve to code information about the physical characteristics of an object (e.g., its roughness).

Electrophysiological studies [76] demonstrated that neurons of the trigeminal complex can be divided into 3 groups. For example, silent (S), low-frequency (LF), and high-frequency (HF) neurons are distinguished based on their spontaneous firing activity patterns [mean spike generation frequency (MSF) in the absence of mechanical stimulation of the vibrissae]. Another classification makes use of neuron responsiveness to stimulation. In the framework of this classification, the responses are categorized into phasic (Ph), i.e., short bursts of impulses closely associated with the beginning or end of the stimulus action (Fig. 5a), and tonic (T), i.e., a sustained train of spikes lasting as long as the stimulus acts (Fig. 5b).

Ongoing studies involving anaesthetized rats are focused on the character of responses of trigeminal complex neurons to the stimulation of the vibrissae by directed short air puffs. Such stimulation causes the most natural movements of the vibrissae. The air was conducted to a selected vibrissa and its neuron responses were recorded when only this single whisker moved. The first series of experiments was carried out at a constant frequency (1 Hz) of stimulation 10, 50, and 100 ms in duration. Reference [80] presented results of a statistical analysis of the percentage ratio of tonic-to-phasic responses in each nucleus, mean spike repetition rate, etc.

The analytic methods used in the study disregard the dynamics of neural responsiveness, i.e., variations of firing activity during the entire period of stimulus action. They are based on the assumption of identical (stereotyped) neuronal responses to similar stimulation. At the same time, the experiments revealed that responses frequently deviated from the stereotype. Therefore, investigation of this effect might shed light on some underlying dynamic and behavioral processes.

We applied wavelet analysis for the estimation of stability of neuron responses to identical stimuli [15]. The database available for the analysis comprised 95 experimental recordings, including 34 files with neuron activation signals from the principal sensory nucleus (Pr5), and 29 and 32 files with signals from the oral (Sp5o) and interpolar (Sp5i) nuclei, respectively. The second series of experiments was carried out at a fixed impulse duration of 10 ms and variation of stimulation frequency from 1 to 30 Hz. The frequency of stimulation was changed randomly every 10 s during each recording, the overall duration of stimulation at a given frequency being 50 s. The data obtained in the second experimental series included 91 recordings (33, 17, and 41 data sets for the neurons of Pr5, Sp5o, and Sp5i nuclei, respectively).

It was taken into consideration in the study of time–frequency dynamics of neuron responses that information is carried by spike generation times, but not shape. Then, it was possible to represent signals of neuron electrical activity $x(t)$ in the form of a train of δ-pulses (Fig. 6a), with each pulse

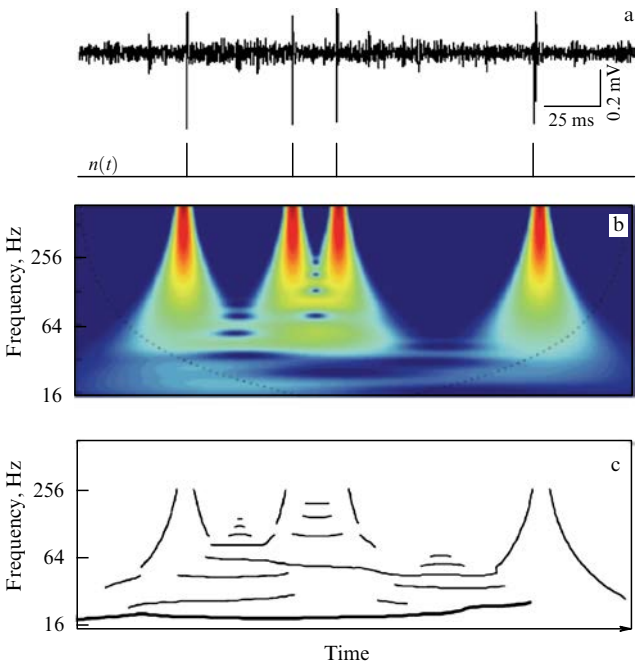

Figure 6. Representation of a neuron activity in the form of a series of δ-pulses (a) and results of wavelet analysis of this signal: energy spectrum (b) and distinguished wavelet transform ridges (c).

corresponding to the moment of generation of the next spike (t_i):

$$x(t) = \sum_i \delta(t - t_i)\,. \tag{21}$$

Representation (21) of the initial process furnishes an opportunity to analytically compute wavelet transform coefficients using the Morlet wavelet:

$$W(a,b) = \frac{\pi^{-1/4}}{\sqrt{a}} \sum_i \exp\left[-\mathrm{i}2\pi f_0 \frac{t_i - b}{a}\right] \exp\left[-\frac{(t_i - b)^2}{2a^2}\right]. \tag{22}$$

Figures 6b, c display the examples of the calculated energy spectrum of a neuron signal and singled out wavelet transform ridges that describe the behavior of instantaneous frequencies by analogy with the results presented in Section 3.1. It appears natural from general considerations to examine neuron responses near the external impact frequency (1 Hz in the first series of experiments). In the case of conventional response (when a neuron generates one and the same characteristic spike sequence per stimulus or stereotype), the instantaneous rhythm frequency in the vicinity of 1 Hz is constant (Fig. 7a). For aperiodic response, such rhythm fluctuates: the stronger the fluctuations, the greater the difference between neuron responses (Fig. 7b).

Quantity $\rho = 1/\sigma_w^2$, where σ_w^2 is the dispersion of the instantaneous rhythm frequency in the vicinity of stimulation frequency, was considered as a quantitative characteristic of response stability. Note that the proposed approach differs from the simple statistical analysis, e.g., the construction of cumulative post-stimulus histograms. By way of example, Fig. 8 shows two spike sequences: (a) periodic (2 spikes per stimulus), and (b) aperiodic. Integrated spike distributions in the two sequences being identical (2 spikes per stimulus on the average), the cumulative post-stimulus diagrams will be very similar and the proposed characteristic taking account of time-dependent neuron dynamics will expose fundamental differences between the two responses.

A peculiar feature of this approach is the analysis of neuronal responses in the neighborhood of the stimulation frequency. In the case of multifrequency responses, e.g., the generation of bundled activity, it allows differentiation between cell electrical activities in terms of frequency and investigation into the firing activity depending on the external stimulus frequency. Let us see what essentially new information on neuronal dynamics may be possibly gained by this approach.

To begin with, we calculated levels of stability ρ for all neurons and three types of stimulation. Thereafter, the type of stimulation (10, 50, or 100 ms) leading to maximum stability of the response (minimum deviation from stereotype during the whole stimulation time) was determined for each neuron. Next we computed the percentage ratio of $\rho_{50} > \rho_{10}$ to $\rho_{50} < \rho_{100}$ neurons to describe qualitative changes in neuronal response stability upon an increase in stimulus duration ($10 \to 50 \to 100$ ms). These data are summarized in Table 1. The maximum stability of responses from the neurons of the Pr5 nucleus stimulated by medium-length impulses (50 ms) was documented for 53% of the cells. In 73% of the neurons, the response to a series of 50-ms stimuli was more stable than to 10-ms air jets ($\rho_{50}^{\mathrm{Pr5}} > \rho_{10}^{\mathrm{Pr5}}$). Similar dynamics was observed for neurons of the Sp5i nucleus where 67% of the cells responded to 50-ms stimulation with maximum stability, while only 8% of them exhibited maximum ρ for responses to

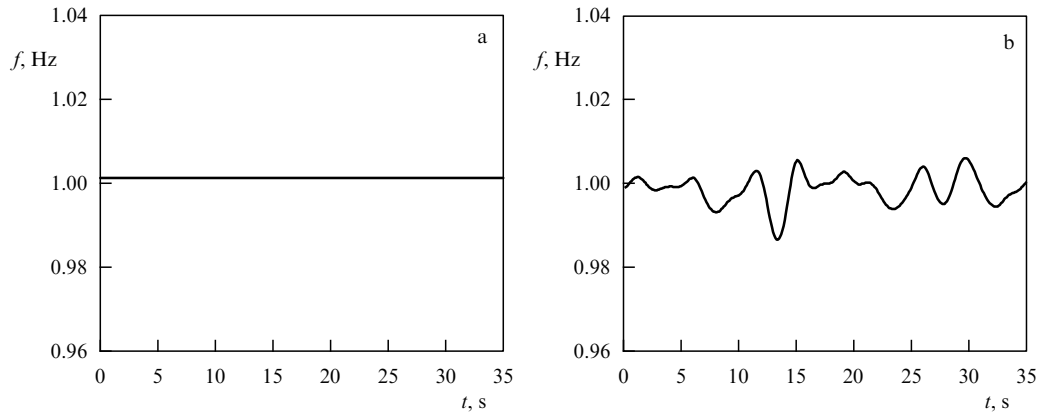

Figure 7. Time dependences of the instantaneous rhythm frequency near 1 Hz for periodic (a) and aperiodic (b) neuronal responses to stimulation (results of experimental data processing).

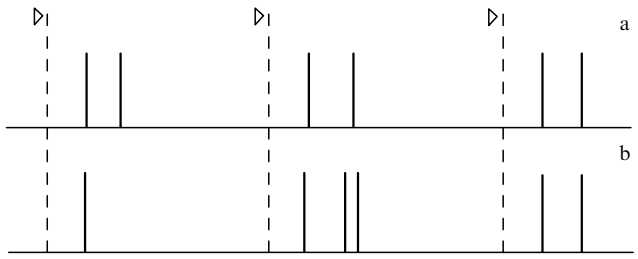

Figure 8. Examples of different responses of two neurons to the same stimulation for which the cumulative post-stimulus histograms are virtually indistinguishable, whereas the values of stability characteristic ρ allow the differences to be exposed. Dashed lines indicate the onset of each stimulus.

Table 1. Comparative analysis of the stability of neuronal responses evoked by sensory stimulation of neurons in the three nuclei.

	Maximum ρ			Increase in ρ upon 10 → 50 ms transition	Decrease in ρ upon 50 → 100 ms transition
	10 ms	50 ms	100 ms		
Pr5	20%	53%	27%	73%	73%
Sp5i	8%	67%	25%	92%	75%
Sp5o	50%	17%	33%	33%	67%

10-ms stimulation. In 92% of the cases, the value of ρ grew as the stimulus duration increased from 10 to 50 ms. Thus, the neurons from Pr5 and Spi5 nuclei are characterized by rather similar responsiveness to variation of the stimulus duration.

A different type of responsiveness was inherent in neurons of the oral nucleus. The maximum stability of their responses was obtained at 50 ms durations for only 17% of the cells. Most neurons (50%) showed the maximally stable response ρ to 10 ms stimulation. The value of ρ increased only in 33% of the cells as the stimulus duration increased from 10 to 50 ms. Thus, the proposed method has demonstrated a substantial difference in the responsiveness of neurons from Pr5, Sp5i, and Sp5o nuclei to stimulation of varying duration.

The above results give reason to speak about markedly different dynamics of neuronal responses in the three nuclei of the trigeminal complex, which is attributable to their anatomical structure and physiological specialization. Indeed, the Pr5 and Sp5i nuclei, in contrast to Sp5o, are characterized by apparent somatotopic organization and have direct thalamic projections. Moreover, the Pr5 and Sp5i nuclei process the major portion of tactile information, whereas the Sp5o nucleus largely transfers painful stimuli supplemented by space–time information. This fact may account for the predominant susceptibility of Sp5o neurons to the shortest (10 ms) stimulation, for which the presence of a stimulus is of greater importance than its characteristics.

This logically suggests that frequency variation of a periodic external action f_{st} can also influence the stability of neuronal response. Under slow stimulation (e.g., 1 impulse/s), a neuron is able to respond to each consecutive stimulus and recover prior to arriving the next one, thus exhibiting the simplest stimulus–response dynamics. At a higher frequency f_{st}, the neuron is likely to miss certain stimuli and have its dynamics disturbed. Therefore, it might be thought that a rise in the frequency f_{st} would results in impaired dynamic stability of the neuronal response. On the other hand, a stimulus of a definite frequency can be regarded as a whole associated with the vibration of a vibrissa palpating a rough surface with the respective spatial frequency. In this case, $f_{st} = f_{sp}v$, where f_{sp} [cm^{-1}] is the spatial frequency, and v [cm s^{-1}] is the speed with which the vibrissa tip palpates the surface. Hence, a given neuron may be tuned to detect a definite frequency; in other words, its response will be maximally stable at this frequency. This assumption is based on the results of numerous studies (e.g., papers [81–83]) suggesting the importance of the frequency parameter of vibrissal movements over the surface for the formation of an adequate tactile image. A sequence of impulses of a given frequency can be perceived as a single complex stimulus. There is a sound reason to expect a different optimal frequency for individual neurons.

Our studies revealed the presence of cells of both types. The dependence $\rho(f_{st})$ may reflect three main variants of behavior (Fig. 9), viz. (a) the occurrence of the 'optimal' frequency of the external action, (b) a monotonic decrease in ρ with growing f_{st}, and (c) a weak dependence of ρ on the stimulation frequency. The first variant is especially common: it was observed in our experiments in 58% of the neurons of the principal nucleus (Pr5), 59% of the nerve cells in the interpolar nucleus (Sp5i), and 53% of the neurons in the oral (Sp5o) nucleus [84]. Type (b) was documented for 33%, 31%, and 35% of the neurons in Pr5, Sp51, and Sp5o nuclei, respectively, and type (c) for 9%, 10%, and 12% of the cells in the respective nuclei. Thus, characteristics of the Sp5o nucleus are slightly different from those of Pr5 and Sp5i. Notice that variant (a) may be interpreted as band-pass filtering of the stimuli, variant (b) as LF filtering, and variant (c) as the absence of frequency dependence of neuronal responses on stimulation.

Statistical analysis of the stimulation frequency at which the maximum dependence $\rho(f_{st})$ is observed for neurons of the first type yielded the following results (mean $\pm$ standard and deviation): 5.1 ± 4.2 Hz (Pr5), 5.2 ± 3.9 Hz (Sp5i), and 4.0 ± 3.8 Hz (Sp5o). Thus, the neurons of the two former nuclei exhibit similar dynamics, whereas the mean frequency of neuronal response stabilization in the oral nucleus is slightly lower.

The existence of the preferred form of the neuronal response to external actions recorded in almost 60% of the neurons of Pr5 and Sp5i nuclei may be related to presenting characteristic time scales in the functioning of nerve cells that we investigated, among other factors, by wavelet analysis in Refs [67, 68]. The observed frequency characteristics fall into the oscillation frequency range characteristic of active palpating movements (4–12 Hz) [85]. Our findings are supported by the data obtained by measuring the amplitude of an averaged neuronal response in the somatosensory cortex (SI), where similar filtration properties were identified [83]. It may be supposed, therefore, that part of the filtration characteristics manifested in neuronal responses of the somatosensory cortex are evoked by an analogous response of trigeminal neurons. We note that the application of statistical methods standard for neurodynamics did not allow discriminating between neuron electrical activities with different frequency characteristics. Instead, we usually observed similar dependences of MSF on the stimulation frequency for the variants presented in Figs 9a, b.

3.3 Wavelet coherence method for the analysis of neuronal responses to sensory stimulation

As mentioned in Section 3.2, the frequency structure of point processes, such as spike trains, may be studied using Fourier

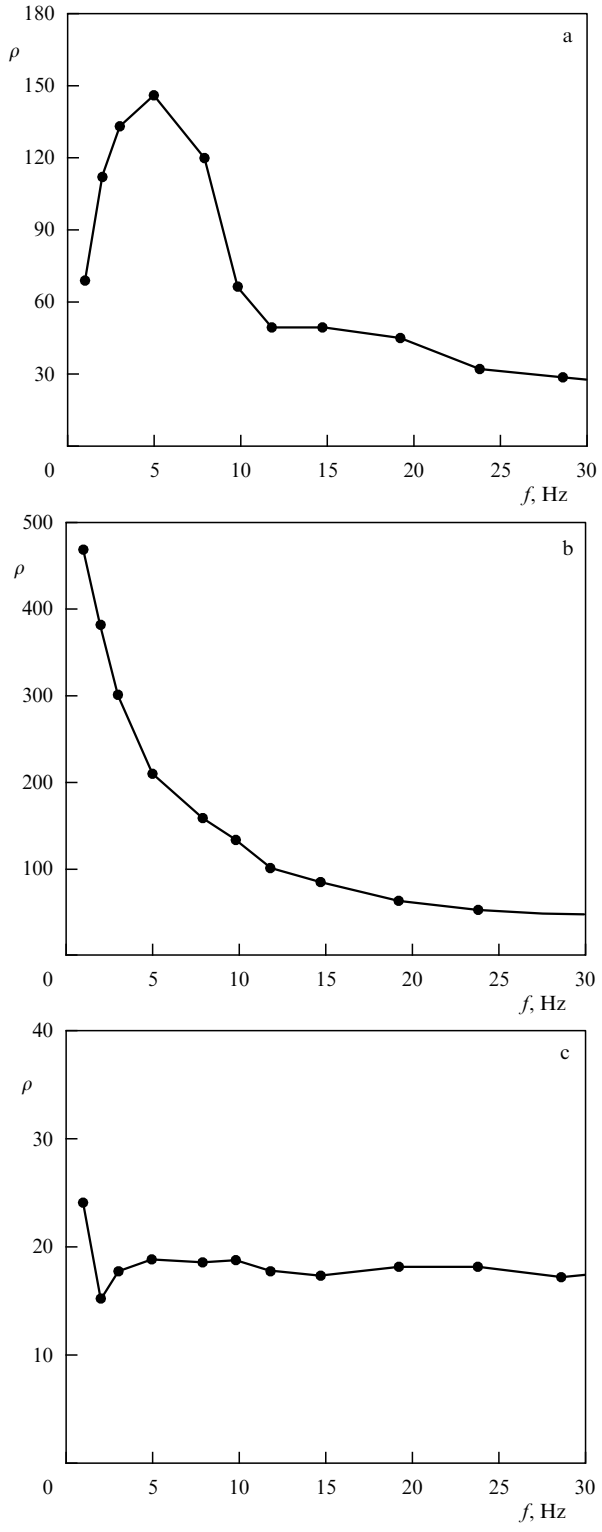

Figure 9. Three main types of the dependence of neuronal response dynamics stability on the frequency of a periodic external action: (a) band-pass stimulus filtering, (b) transmission of low frequencies, and (c) the absence of apparent frequency dependence.

analysis. However, such an approach has a number of limitations hampering the assessment of neuronal responses to stimulation [74]. The attraction of a concept of wavelets is an alternative variant of spectral analysis of neural system dynamics.

The wavelet spectrum $W(a,b)$ of a spike train can be computed by formula (22). It is convenient to employ a variant of energy spectrum normalization taking account of the mean spike generation frequency r [86]:

$$E(a,b) = \frac{1}{\sqrt{\pi}\, r f_0} \left| W(a,b) \right|^2 . \tag{23}$$

In this way, the unit energy of a 'random' spike sequence (i.e., one with a random distribution of interspike intervals) is obtained uniformly distributed over all scales: $\langle E(a) \rangle_b = 1$. The global energy spectrum can be derived by averaging (23) over time T during which a neuronal response is generated:

$$E(a) = \frac{1}{T} \int_0^T E(a,b)\, \mathrm{d}b . \tag{24}$$

When studying the dynamics of two consecutive spikes N and M, it is possible to introduce in the consideration, by analogy with the Fourier cross spectrum, the wavelet cross spectrum

$$E_{\mathrm{NM}}(a,b) = \frac{W_{\mathrm{N}} W_{\mathrm{M}}^*}{f_0 \sqrt{\pi r_{\mathrm{N}} r_{\mathrm{M}}}} . \tag{25}$$

In this case, the normalized measure of the interrelationship between two spike sequences is wavelet coherence [54, 55, 87]

$$C_{\mathrm{NM}}(a,b) = \frac{\left| S\left[E_{\mathrm{NM}}(a,b)/a \right] \right|^2}{S\left[E_{\mathrm{N}}(a,b)/a \right] S\left[E_{\mathrm{M}}(a,b)/a \right]} , \tag{26}$$

where S is a certain smoothing operator [87]. A numerical estimation of measure (26) can yield erroneously high values of coherence in the case of vanishingly small values of the energy of one or both signals (i.e., at $E(a_*, b_*) \simeq 0$). In order to obviate this problem, the value of C_{NM} is equated to zero if the current energy value of at least one signal becomes lower than a certain threshold level.

Two linearly independent spike sequences are characterized by the small value of coherence $C_{\mathrm{NM}}(a,b) \simeq 0$, whereas $C_{\mathrm{NM}}(a,b) = 1$ corresponds to the strict linear interrelationship between spike trains on scale a at time $t \approx b$. When a time sequence of stimuli is used as one of the spike sequences, the measure (26) can be employed for the assessment of functional interdependence between stimulation and neuronal response. In periodic stimulation with frequency f, it is appropriate to focus attention on time scales a in the vicinity of the stimulation frequency.

Let us consider an example of the application of the wavelet coherence concept for the study of neuronal responses to tactile stimulation in rat experiments. We chose an experimental recording of a spike sequence containing the following three regions: I — spontaneous neuronal activity; II — control tactile stimulation (32 s) in the sensitive region of neurons of the *nucleus gracilis* using a solenoid to perform periodic pulsed stimulation (31 impulses with a frequency of 1 Hz and of 20 ms duration each), and III — analogous tactile stimulation following additional electrical stimulation of the somatosensory cortex. Figure 10a shows the respective sequences of the stimuli and neuronal responses. Results of the wavelet analysis of neuronal signals (using the 'mother' Morlet wavelet) are presented in Fig. 10b depicting irregular neuronal activity. The spontaneous dynamics mode (no stimulation, region I) lacks dominant rhythmic processes.

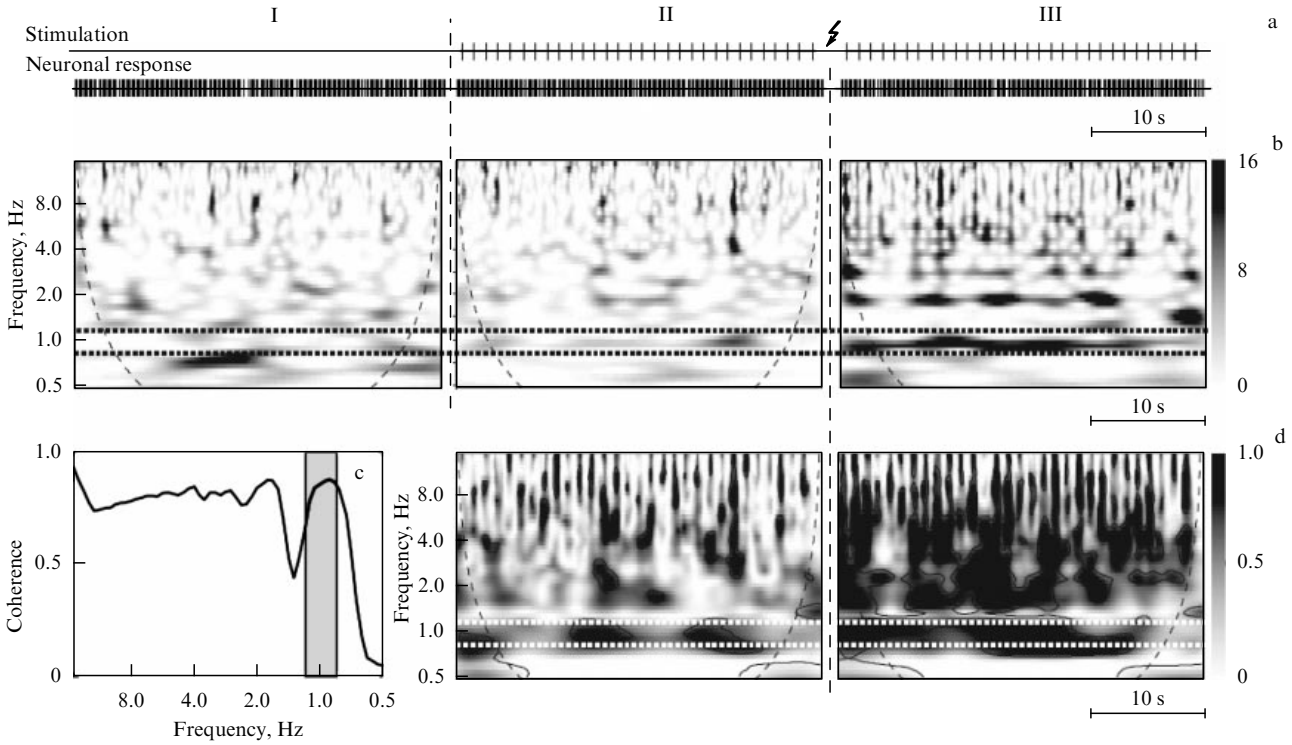

Figure 10. An example of wavelet analysis of a neuronal response to stimulation. (a) Three regions corresponding to stimulation and neuronal response: I — spontaneous firing activity; II — control tactile stimulation, and III — tactile stimulation following additional electrical stimulation of the somatosensory cortex. (b) Calculated wavelet energy spectra (23) for the respective regions. (c) The level of statistical significance for the calculation of wavelet coherence reached by surrogate data analysis. (d) Computation of the wavelet coherence measure (26).

Region II displays a spectral peak in the vicinity of the stimulation frequency (within a 0.83–1.16 Hz range), the boundaries of which are indicated by horizontal dotted lines. This peak is indicative of a stimulus-induced rhythmic neuronal response. However, the peak amplitude varies with time and undergoes low-frequency (below 0.3 Hz) oscillations, suggesting that neuronal responses to periodic stimulation are not identical in time, i.e., a neuron responds to similar stimuli by different spike trains with different durations of spike-to-spike intervals. The spectral peak near the stimuli frequency becomes more prominent after electrical stimulation of the somatosensory cortex (region III). Slow oscillations of the peak amplitude become weaker but remain in the structure of the signal being analyzed. Moreover, the energy of oscillations of stimulation frequency harmonics increases.

This picture emerges from the results of a qualitative analysis of the wavelet spectrum of the neuronal response to stimulation. A quantitative analysis of the repeatability of neuronal responses to stimulation was performed by calculating the wavelet coherence (26) of stimulating impulse trains and neuronal spike sequences. The statistical significance of the degree of coherence determined in this way was estimated in a statistical test based on the generation of surrogate spike sequences by random mixing of interspike intervals (phase relations for two signals). Figure 10c presents a statistical significance curve corresponding to level $p = 0.05$ for the neuronal response frequency range of interest. The values of the coherence measure (26) above this curve were considered statistically significant.

Figure 10d gives the calculated results of wavelet coherence of tactile stimulating impulses and induced neuronal responses. Because tactile stimulation is periodic (contains a single frequency), the analysis of response coherence must take into account only the frequency range near the stimulation frequency (indicated by dotted lines in Fig. 10d). Control stimulation resulted in three regions of statistically significant coherence in this frequency range (Fig. 10d, left), reflecting the action–response interrelationship. However, this interrelationship is not constant. The coherence measure (26) increases considerably after electrical stimulation of the somatosensory cortex (Fig. 10d, right). A more detailed study undertaken in Ref. [86] revealed for the first time two phenomena: (1) the degree of the functional relationship between the stimulation and the response increases after electrical stimulation of the somatosensory cortex, and (2) the coefficient of the functional relationship is a dynamic characteristic slowly oscillating in time. In certain regions of experimental recordings the value of this parameter lies below the statistically significant level, suggesting a temporary loss of the stimulus–response interrelation for a single sensory neuron.

The authors of Ref. [86] estimated the probabilities of different types of changes in neuronal response coherence in *nucleus gracilis* under the effect of electrical stimulation of the somatosensory cortex. In most cases (59%), the stimulation enhanced the coherence of responses to tactile stimulation. Neuronal responsiveness remained unaltered in 24% of the cases, while coherence decreased in 17% of them.

4. Analysis of extracellular electric potentials and the problem of spike sorting using wavelet-based methods

Investigations into the principles of coding information by neurons and their assemblies have been largely confined to the accumulation of experimental data on the reaction to one

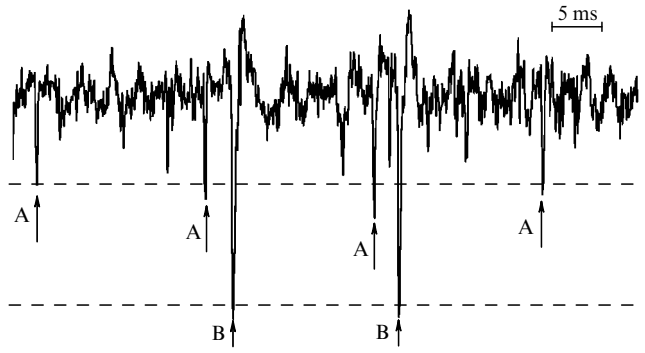

Figure 11. An example of an extracellular electric potential containing several spikes differing in shape and amplitude. The spikes labelled by different letters (A and B) were generated by two different neurons.

type of stimulus or another. Traditionally, the extracellular electric potential is recorded to study the dynamics of cell firing in a certain local region near the microelectrode. The recorded potential represents an integral electrical activity of a neuronal assembly. In order to experimentally investigate the activity of individual neurons, the spikes need to be sorted on the basis of their shapes.

It is traditionally assumed when addressing the problem of spike identification (classification or sorting) that each neuron generates spikes of identical shapes and amplitudes, and the spike shape is unique for a given neuron, being predetermined by its morphology and the site of recording (close to the axon, soma, etc.), while the spike amplitude depends on the distance between the cell and the microelectrode. Such an assumption is not always justified (e.g., for spikes in a bundle of impulses) but is logical, bearing in mind that the natural variation of the shape of the action potential of a single neuron is often inappreciable compared with the difference between the spikes of the adjacent cells. Therefore, the issue of spike identification is theoretically reduced to the extraction of a few sequences of similarly shaped spikes (supposedly generated by one neuron) from the experimental data (Fig. 11). Ideally, in the space of characteristics describing the spike shape, clusters must form corresponding to the spikes of individual neurons. Given that a number of clusters are distinguished and separated from one another, the issue of identification can be regarded as successfully resolved.

In practice, however, this is technically difficult to accomplish in the presence of significant background noise added to the signal and leading to various distortions of the spike shape. The noise may be of a different nature (e.g., formed by the electrical activity of the distant cells or by the measuring and transmitting equipment), and its spectrum may overlap the signal spectrum of interest, which significantly complicates frequency filtering. Taken together, these factors inevitably lead to identification errors. The error level estimated for extracellular electric signals in the presence of strong background noise may be as high as 50% [88].

Identification of spike sequences is also possible by visual comparison of their shapes and by manual grouping. Admittedly, this approach is inefficient because the recordings may contain several hundreds (or several thousands) of spikes, which makes their visual sorting very difficult. Hence, the necessity of automated sorting of spikes into groups.

4.1 Methods for classification of neuronal spikes

The issue of automated spike identification is dealt with in numerous publications (see, for instance, Refs [89–93]). The simplest way to address this issue is to discriminate between the spikes on the basis of their amplitudes (threshold sorting). The amplitude (or height) of the action potential decreases with increasing distance between the cell and the recording electrode. If this distance is very small, the amplitude of generated spikes will be much greater than the amplitude of spikes from remote cells and the background noise. In this case, at least one type of spikes is possible to identify using a threshold device (trigger). Impulses having different amplitudes are separated by setting specific threshold levels (see Fig. 11). An advantage of this approach lays with minimum hardware and software requirements, real-time performance, and sufficiently accurate, in a number of cases, information sought by the experimentalist. An obvious drawback of the threshold sorting method is far from always adequate group separation of signals with similar amplitudes. For example, this method is inapplicable to discriminate between waveforms depicted in Fig. 12. Also, instrumental detection does not allow acceptably accurate differentiation of the signal from background noise and interference.

The principal component analysis (PCA), a variant of factor analysis, is considered the most effective tool among numerous currently available classical methods for automated spike sorting [88]. It has been successfully applied to image recognition and compression, noise suppression on images, reduction of dimensionality in dynamic models without substantial loss of informative value (e.g., in the description of turbulence), etc. The idea behind this method is to search for a set of orthogonal functions characterizing the most important shape peculiarities of the signal. From the standpoint of computational mathematics, the problem reduces to the search for eigenvectors (so-called principal components) of the covariance matrix constructed on the base of experimental data, i.e., all impulses whose minima or maxima occur simultaneously. Each spike $x(t)$ can be represented as the sum of the principal components with the corresponding weight coefficients S_i. The weight coefficients are defined as

$$S_i = \sum_t p_i(t)\, x(t)\,, \tag{27}$$

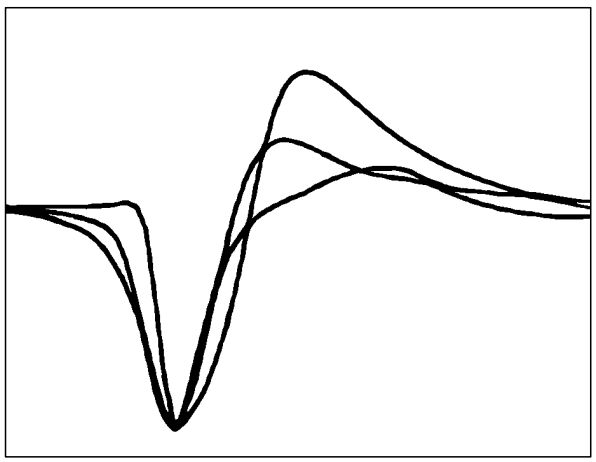

Figure 12. An example of waveforms generated by three different neurons.

where t is discrete time, and $p_i(t)$ is the principal component with number i. The weight (or scaling) factors S_i are used as characteristics in spike sorting. The most important information is usually contained in a few first principal components describing the main peculiarities of the spike shape (they are utilized to diagnose the main differences between spike types). The scale coefficients of the first two principal components ensure much more accurate separation of spikes than simple threshold methods [88]. The disadvantages of PCA are less apparent than those of the threshold sorting technique.

A new approach to spike identification based on the analysis of wavelet transform coefficients has recently come into use. Its advantages over standard methods have been demonstrated in a number of studies [22–24]. For example, in the wavelet-based spike classifier (WSC) method [22], discrete wavelet transform coefficients obtained in the framework of the pyramidal algorithm [94] are employed as a quantitative measure in sorting neuron action potentials. The main problem with this method is the choice of wavelet transform coefficients most essential for the separation of different types of impulses. Maximum mean and mean-root-square deviations of wavelet transform coefficients were used in Ref. [22] as an appropriate criteria. However, this method is not strictly substantiated, and there is no universal approach to the choice of the 'right' coefficients. In practice, different variants of characteristics have to be analyzed with the aim of using them for the recognition of signal shapes. Formally, both DWT and CWT can be applied for the purpose. The former approach appears more attractive by virtue of the high computation speed. The latter method in view of its redundancy inspires hope that while moving over the scale parameter with a small step one can study in more details how transform coefficients depend on the observation scale at any instant of time. In this case, more descriptive results can be obtained at the penalty of a loss in operating speed; they at least may be used to elaborate practical recommendations for the choice of characteristics required in recognition of spike shapes, which could be useful in the future for the application of a faster algorithm of DWT-based recognition.

Although wavelet analysis is potentially a more powerful tool than PCA, there are some obstacles to its practical implementation; the two following are worth mentioning as among the most important:

(1) Obviously, the results of analysis, i.e., wavelet transform coefficients, depend on the choice of the basis function. There is no unambiguous answer to the question of how to choose the wavelet in each concrete case. Thus, the efficacy of the method depends on the form of the signal obtained in the experiment. On the other hand, the employment of different basis functions permits making the signal recognition algorithm more flexible and accurate.

(2) The calculation of wavelet transforms for experimental data yields a set of coefficients characterizing each action potential (up to 64 coefficients are usually considered for neuronal spikes in the case of DWT) [22]. These coefficients are unsorted, as in PCA: hence, the question of which coefficients to chose as characteristics for signal identification.

The choice of coefficients has a stronger influence on the results of analysis than the choice of the basis function. Various procedures have been proposed in the literature, from the estimation of maximum dispersion, maximum mean value, and multimode distribution to more complicated approaches based on the theory of information [22–24]. Each of them has specific disadvantages. The maximum mean value and dispersion testify that a given wavelet transform coefficient contains important information about the signal, but it does not guarantee that such an approach will lead to reliable discrimination between two different waveforms. The multimode distribution is a necessary condition for successful spike sorting, but many of the sets of coefficient values may follow such a distribution, and it is difficult to decide how to optimally choose between them. This problem is of special importance when the experimental data contain impulses of both rather similar and very different shapes. In the case of the arbitrary choice of coefficients, markedly different signals can be separated with a high degree of certainty, but it is very difficult to discriminate between similar ones. It is due to the wrong choice of coefficients and the lack of a universal approach to the optimal choice that the efficacy of wavelet transform-based methods may prove lower than that of PCA.

Our publications [95, 96] provide examples of successful and unsuccessful applications of wavelets for addressing the issue of automated spike separation. It was revealed that the use of wavelets is especially efficacious in the case of a small-scale structure, i.e., differences in the waveforms of the spikes from adjacent neurons manifested on small scales (PCA can ignore such differences) and at a high level of low-frequency fluctuations in extracellular recordings of electric potentials. Nevertheless, the optimal choice of wavelet transform coefficients for spike sorting remains a challenge that hampers the recognition of different waveform types.

We proposed the following approach to resolve this problem. Suppose that standard PCA makes it possible to obtain clusters in the space of characteristics that are situated close to one another. It would lead to appearing numerous identification errors in cluster overlap regions. Figure 13a illustrates such a situation that emerged from the analysis of the experimentally recorded extracellular electric potential. Two clusters correspond to the spikes of two neurons, but there is no distinct boundary between them because of the presence of background noise.

In order to reduce the number of identification errors, a special method was proposed based on a combination of wavelet analysis and classical PCA [wavelet shape-accounting classifier (WSAC)]. Such integration ensures a better separation of clusters than either of the two methods used alone.

The **first step** of the WSAC algorithm consists in a search for *characteristic signal shapes*. To this end, PCAs of all experimental spikes are utilized. Then, spike shapes are averaged in the small neighborhood of each cluster's center; this procedure yields two averaged forms of signals (Fig. 13a, insets). They are localized in the cluster centers and therefore may represent 'real' spike profiles of two different neurons, minimally subject to the influence of noise (the greater the influence, the farther away the point lies from the center).

Step 2 implies the wavelet analysis of the averaged signal shapes obtained and the search for wavelet transform coefficients that best of all demonstrate the differences between them. To this end, an analysis is performed in a wide range of scales and shifts. Then, the difference between the respective values of wavelet coefficients is estimated and maximally different coefficients are chosen. In other words, we search for wavelet transform coefficients with regard to individual features of concrete impulse shapes rather than in an arbitrary fashion. Figure 13b illustrates the scale dependences of the difference between all the values of wavelet

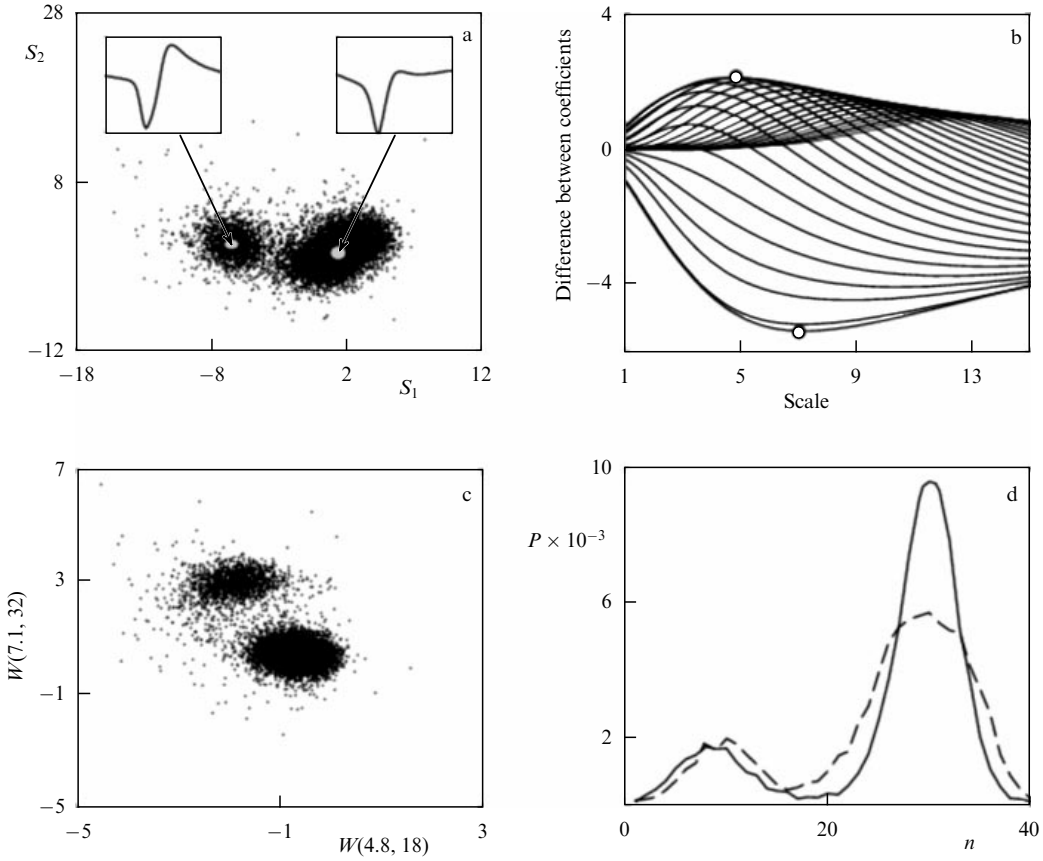

Figure 13. Illustration of the proposed WSAC method for improving spike identification based on the shape of the action potentials. (a) First step. Two overlapping 'clouds' of points corresponding to impulses of different types were obtained in the space of scale coefficients by PCA. The insets show characteristic impulse shapes obtained by averaging the signals corresponding to the points near cluster centers. (b) Second step. Scale-dependent difference between wavelet transform coefficients of two characteristic impulses. The circles label a pair of maximally different coefficients ($a = 4.8$, $b = 18$ and $a = 7.1$, $b = 32$). (c) A new space of characteristics for the chosen wavelet transform coefficients. (d) Point distributions in the space of characteristics for PCA (dashed line) and the proposed method (solid line).

coefficients for CWT (each curve corresponds to a definite value of the shift parameter, and the 'mother' WAVE-wavelet constructed based on the first derivative of the Gaussian function is chosen as the basis function [29, 32]). Two points corresponding to extrema of these dependences are labelled at the bottom and top of the figure. It should be emphasized that in certain cases a few extrema appear on different scales and the number of characteristics that can be used for identification increases. As a result, we will have a set of 'optimal' coefficients reflecting the most important differences between the averaged signal shapes. This procedure allows a better separation of clusters than PCA because differences are sought for concrete impulse shapes rather than from general considerations.

In the **third step** of the algorithm, the chosen wavelet transform coefficients are calculated from experimental data for all impulses, and the values thus obtained are considered to be characteristics suitable for identification (Fig. 13c). This procedure allows the clusters to be better separated from each other.

Figure 13d depicts point distribution densities in the space of characteristics for PCA and the proposed method. The principal maximum of the probability density function for wavelet analysis shrinks and becomes more conspicuous than that obtained in PCA. This circumstance makes it possible to much better separate the two clusters and reduce identification errors arising mainly in the intercluster region. In this case, the arbitrary choice of wavelet transform coefficients (as recommended in Ref. [22]) does not permit improving identification vis-à-viz the PCA.

The proposed approach is applicable both in the case of CWT, where it yields more descriptive results in the form of smooth dependences of coefficient differences (Fig. 13b), and in the case of DWT; the method remains essentially the same, but the DWT algorithm has an obvious advantage due to the high computational speed.

The approach proposed was tested utilizing surrogate data derived from real experimental signals (over 20 recordings of extracellular electric potential). Each surrogate signal was constructed by choosing two experimental records, one of which contained a group of spikes well separated from the background noise and other action potentials. These spikes were artificially 'cut out' and added in a random manner to the second experimental signal. On the one hand, this preserved all characteristics (noise level and statistics, intrinsic waveform variations, etc.). On the other hand, we obtained *a priori* information on the 'added' spikes belonging to an individual cluster. This *a priori* information allows identification errors to be calculated for a given cluster, and the efficacy of different sorting techniques to be compared.

Figure 13 presents the results for one of the signals containing 16,568 spikes, including 3069 artificially added

Table 2. Spike identification errors in four recordings of neuronal activity obtained using PCA, WSC [22], and the proposed combined WSAC algorithm. The values are percentages of the total number of spikes.

	Signal 1	Signal 2	Signal 3	Signal 4
PCA	9.5	53.4	2.7	6.3
WSC	13.3	48.0	9.6	5.9
WSAC	5.9	34.6	2.1	5.6

ones. The employment of three principal components resulted in 290 sorting errors. Following the recommendations of Ref. [22] for identification by the WSC algorithm, we chose wavelet transform coefficients with maximum standard deviations, maximum values, and bimodal distributions. In this case, the identification error was greater than with the PCA (410 falsely identified spikes). This shows once again that the unjustified choice of wavelet coefficients hampers automated recognition of neuronal activity signals. The proposed algorithm reduces here the occurrence of errors to minimum (there were only 185 misidentified spikes).

Table 2 gives the results of an analysis of four typical signals obtained with the CWT procedure in the framework of the proposed method. In examples 1 and 3, PCA proves superior to WSC, while the proposed WSAC algorithm ensures minimal error in automated identification of impulse shapes. The situation reverses in the fourth case: WSC outperforms PCA and the proposed WSAC approach also has certain advantages. In example 2, all methods are fraught with gross errors due to the high level of background noise, but wavelet approach also proves possible to substantially reduce the number of misidentified spikes by virtue of the optimal choice of wavelet transform coefficients.

4.2 Use of wavelets in combination with methods of artificial neural networks

Another option for devising integrated methods for automated recognition of signal shapes is based on a combination of wavelets and artificial neuronal networks. The neuronetwork technique for signal identification [97–100] has some peculiar features. The scientific literature contains examples of the architectonics of neural networks designed for the above purpose. However, each concrete problem has individual peculiarities of its own and requires correction of the method to be addressed. Not infrequently, the involvement of an autonomous neural network fails to provide the worked-out solutions. Therefore, neural networks are usually integrated into multistep systems for data processing, where each network plays a definite role and thereby contributes to the final result. Because signals of similar shapes have to be distinguished in the presence of background noise, an algorithm is needed that first is sensitive enough to identify signals, second is efficacious despite the presence of noises with different statistics, and third has the potential for modification to operate with concrete experimental data.

The problem of neuronal spike identification can be addressed using an algorithm integrating wavelet analysis and the neuronetwork technique. Wavelet transform is an excellent tool to search for characteristic impulse shapes (i.e., for preliminary processing) and to convey this information to the neural network for further treatment. In the next step, an image recognition algorithm is employed.

If signals containing a set of characteristic signs of certain images are sent to the input of a many-layer neuronal network with direct signal propagation [100], it will be able to sort out

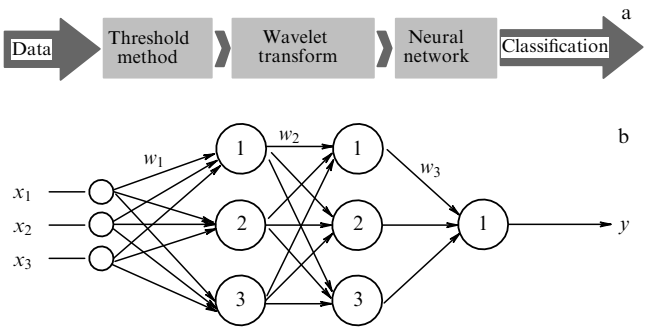

Figure 14. (a) The structure of the method based on the combination of wavelet analysis and neural network technique. (b) The structure of a many-layer neural network with direct propagation of the signal.

these data provided the learning information is available. The learning algorithm for such a network suggests the presence of a training sample and its reference values to be obtained at the output (a so-called learning algorithm with a teacher). In other words, impulse shapes unaffected by the noise present in the experimental recording must be known for the successful operation of the network and spike identification; then, the work of the network reduces to spike grouping.

Figure 14 illustrates the structure of the proposed method. A few steps of data processing may be distinguished.

(1) Experimental data are treated by the threshold method to reveal spikes to be sorted out.

(2) The spike sequence obtained is subjected to discrete wavelet transformation by the pyramidal algorithm. It gives a set of wavelet transform coefficients for each spike (in our calculations it contained 64 points). The Daubechies wavelet (D^8) was used as the 'mother' wavelet.

(3) Wavelet transform coefficients characterizing the noise component of the signal (i.e., those corresponding to small amplitudes) are eliminated, and the values of the remaining coefficients are delivered to the input of the neural network.

(4) After data arriving at the input of the neural network, it sorts the spikes into groups and constructs their classification in the space of characteristics. The logistic function is used as the network activation function.

In our study, we chose a three-layer neural network with direct signal propagation (Fig. 14b) — one of the many possible configurations. However, the following needs to be taken into consideration. The network with direct signal propagation or multilayer perceptron shown in Fig. 14b [99] is a well-studied basic one. The choice of the number of neuronal layers and the number of elements in each of them is based on the known plasticity–stability dilemma [97]. Evidently, the more complicated the network organization in terms of the total number of elements, the greater the adaptive potential of the system. However, adaptivity may lead to instability. Therefore, structurization of the neural network must ensure both stability and flexibility of its performance.

The proposed method was tested to verify its efficacy and, in particular, assess the influence of background noise statistics on the quality of automated signal identification by the proposed algorithm. Two different spike shapes minimally affected by noise (each containing 64 readings) were extracted from the experimental data (extracellular recordings of the activity of small neuron groups). Multiple repetition of the corresponding impulse shapes produced a

test surrogate signal composed of 1892 spikes (with 946 impulses of each type). The spike sequence thus obtained was supplemented by a color noise generated by band-pass filtering of the normally distributed random process. The neural network consisted of three layers, with the input layer containing 64 elements (the number equal to the input vector size), the second layer 32, and the output layer 2. The network had to be learned to enable it to identify a spike with a minimum error after signal decomposition coefficients x_i arrived at the input layer, and to be weakly sensitive to the influence of noise statistics. An error back-propagation algorithm was applied for this purpose [97].

The network training sample x_i was composed of 100 images in the form of wavelet transform coefficient values corresponding to the shape of the first impulse, and 100 images corresponding to the shape of the second impulse. Accordingly, the learning method included 100 stages. The network was expected to achieve the highest-quality separation of spike groups in the space of characteristics. To this effect, the vectors with a set of coordinates in the form of the respective wavelet coefficients for the first and second impulse shapes in a given space were specified as the reference output values y_i. Thus, the neural network having received the input vector containing wavelet coefficients of the first and second impulse images had to associate it with, say, $[0.1; 0.1]$ and $[0.5; 0.5]$ coordinate vectors, respectively. Once this procedure was completed, the neural network was regarded as learned. The network performance was checked by delivering the initial sequence of wavelet coefficients of noise-free spikes to its input. Calculations showed that such a method permits various forms of action potential to be identified as effectively as the standard approaches.

Attention should be given to the following important circumstance. In test experiments with artificially generated data, noiseless impulse shapes and the number of groups of signals being identified are known. Due to this, learning algorithms with a teacher can be successfully used to train neural networks, with both the training sample and the reference data to be obtained at the output being available. The learned neural network capable of classifying impulses within the scope of a concrete numerical experiment is brought about on the base of these data. Real neurophysiological data do not usually contain information about noise-free signals and the number of different kinds of spikes. In this case, the main obstacle to the application of the integrated wavelet analysis/neural network method is network learning. The above reasoning suggests the necessity of modification of the algorithm under consideration by performing the following sequence of actions.

(1) The use of the threshold method to extract spikes for their subsequent sorting.

(2) Preliminary classification by PCA and WSC, obtaining the clustering picture in the space of characteristics.

(3) Finding regions of enhanced point density in the clusters obtained and spike shapes corresponding to these points (closest to noiseless signal shapes).

(4) Wavelet transformation of extracted impulses, obtaining a set of wavelet transform coefficients.

(5) The use of these coefficients as a training sample for the neural network.

(6) Wavelet transformation for the original signal, and analysis of experimental data by the learned network.

Thus, training samples for a neural network are composed of spikes corresponding to the central parts of various clusters, obtained by different automated identification methods, such as principal component analysis or standard wavelet analysis. It is natural to use vectors of coordinates in the space of characteristics as reference values at the network output. As the practice implies, the point pattern on the plane of characteristics obtained by applying automated signal recognition methods (PCA or wavelet analysis) is sometimes ambiguous. Clusters on the plane of characteristics, corresponding to diversified groups of spikes, can be situated close to one another and overlap; as a result, points of one cluster erroneously occur in another, as illustrated by Fig. 15 showing the results of clusterization by wavelet analysis and the proposed wavelet transform method added with a learning neural network. Our studies have shown that this integrated technique permits reducing identification error due to an individual approach to a concrete problem, i.e., to increasing the distance between clusters at the plane of characteristics (see Fig. 15). The individual approach is possible because neural network learning is carried out using a sample that contains spikes extracted directly from the experimental data available for the analysis.

The efficacy of the combined wavelet analysis/neural network method under real conditions was estimated from the analysis of neurophysiological data (experimental recordings of trigeminal complex neuron dynamics). The resultant clustering pictures are presented in Fig. 16.

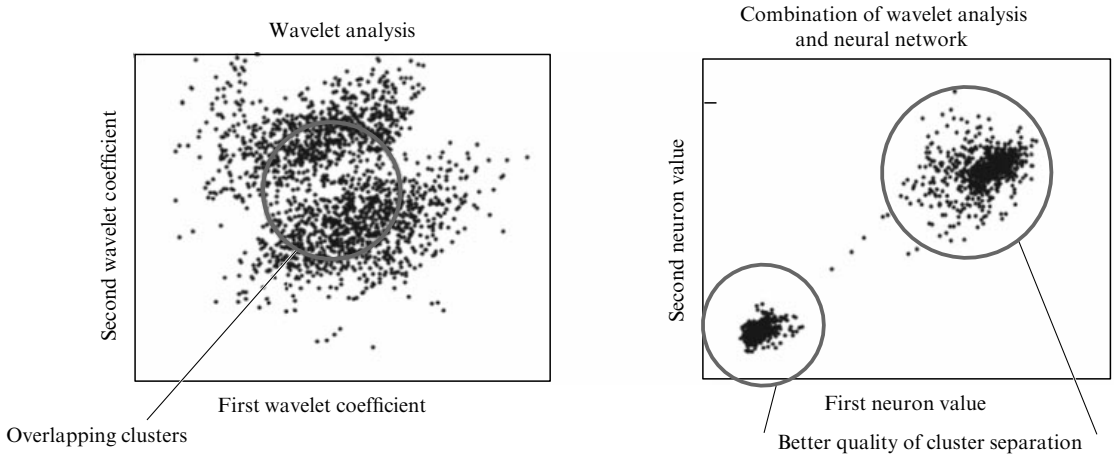

Figure 15. An example of clusterization by a combination of the wavelet transform and neural network.

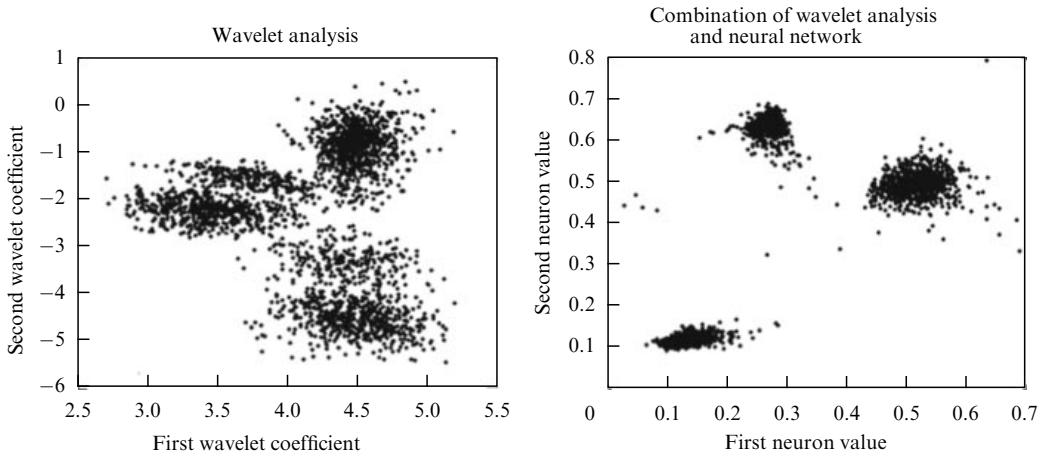

Figure 16. Clusterization picture obtained by the combined wavelet analysis/neural network method for real experimental data.

Figure 16 demonstrates that the use of standard wavelet analysis for data sorting brings forth an illegible clustering picture. The experimental sequence contains three groups of spikes, but clusters are poorly separated and have common points that can be erroneously referred to a group to which they do not actually belong. Following the above algorithm, 50 points were chosen from the centers of the clusters obtained and the resultant sample served to learn the neural network. When the training was completed, a number of values of wavelet transform coefficients of the initial impulse sequence were delivered to the input of the network. The resultant clustering pictures clearly demonstrate a better separation of the clusters, i.e., an improvement in automated signal recognition.

Although this variant of the combined waveform recognition algorithm sometimes permits significantly reducing errors of automated signal recognition, it is also not free from drawbacks. On the one hand, it is superior to utilizing traditional artificial neural networks due to the integration of efficacious time–frequency analysis of signals (wavelet transform) into the image recognition algorithm that allows all the advantages of wavelet analysis to be exploited. In this context, wavelets constitute a stage of preliminary analysis designed for a neural network to choose characteristic signs for better separation of signals from different objects. On the other hand, the variant of signal identification being discussed does not envisage a change in wavelet transform parameters (scale and displacement) at the stage of neural network learning. For this reason, the efficacy of the method depends on the initial choice of these parameters, i.e., the stage of preliminary data processing. This relationship is lost at network learning stage and the situation cannot be repaired at the subsequent stages if the unsuccessful parameters were chosen. It frequently compromises the final stage of the image recognition procedure because such factors as the researcher's experience with the choice of the 'needed' wavelet transform coefficients start playing a role. In order to reduce the influence of the human factor in automated spike sorting, the classical stage of learning (the choice of weight coefficients) needs to be extended by inclusion of an additional tuning of the wavelet transform parameters depending on the accuracy of the solution to the classification problem. It is this approach that is applied in the framework of so-called wavelet neural networks (WNNs) [53, 101–104].

WNNs are structurally and analytically analogous to traditional artificial neural networks, where part of the neurons are substituted by 'wavelet nodes'. In this case, WNN can be treated as an extended perceptron composed of two parts: the wavelet transform to reveal characteristic features of the signals, and an artificial neural network to recognize images on the base of the detected features. The first part includes 'wavelet nodes' in which wavelet functions (e.g., the Morlet function) are used instead the classical logistic function. These wavelet functions allow peculiarities of the signal shape to be determined on different scales. The first part of the algorithm yields a set of coefficients reflecting characteristic features of the signals. These coefficients provide the input signal for the second part of the algorithm, where images are eventually recognized. An essential feature of WNNs is the possibility not only of correcting weights during learning but also of choosing wavelet transform coefficients for the more reliable classification of input signals. A distinctive feature of WNNs is complete integration of procedures for the choice of characteristic signs and subsequent signal recognition in the framework of a single structure. We believe that the exploitation of wavelet neural networks is currently one of the most challenging approaches to solving the problem of image recognition.

5. Analysis of the electroencephalogram by the methods of continuous wavelet analysis

Let us take the next step in the evaluation of possibilities for the application of wavelet analysis in neurodynamics and neurophysiology by moving to the consideration of different aspects of analysis of oscillatory rhythmic processes in the brain. It is a most complex structure composed of a huge number of elements — neurons — each with its own complicated oscillatory dynamics integrated into networks with an intricate topology and numerous interconnections [1, 2, 5, 105–109]. Electroencephalography is a traditional highly effective method for the study of brain electrical activity. An electroencephalogram (EEG) makes up the averaged sum of electric fields generated by synaptic currents of a large group of neurons in the neighborhood of the recording electrode. Analysis of an EEG permits revealing the relationships among various brain regions, elucidating the mechanisms and peculiarities of formation of different types of rhythmic

activity, and in the upshot better understanding the principles of brain functioning as a whole.

An EEG displays a variety of rhythms and periodic oscillations, the frequency of which is an important characteristic of the functional activity of neural structures [105, 110–113]. The development of methods for the investigation of various types of rhythmic activity is of great importance for basic research on brain cognitive functions. It is equally important for applied studies, specifically for the development of new diagnostic methods and analysis of the brain functional state, monitoring its pathological activity in medical practice (e.g., in epilepsy or Parkinson's disease), and the creation of specific brain–computer interfaces [114–121].

As discussed in Sections 2–4, the mathematical apparatus of continuous wavelet analysis is well suited for describing nonstationary signals whose spectral composition and statistical characteristics vary in time. The following important features are worth mentioning:

(1) it reveals the time-frequency structure of signals, thus allowing localization of their peculiar features in time and frequency domains are worth mentioning;

(2) it enables efficacious analysis of short-term time series containing a small number of characteristic oscillation periods;

(3) it provides flexibility in the choice of the basis functions into which a signal is expanded, thus allowing taking account of peculiarities of the data being analyzed;

(4) it ensures a highly effective analysis of noisy data (i.e., signals considered the sum of a meaningful signal and noise).

All these peculiarities need to be taken into consideration in analyzing EEG signals, bearing in mind the following properties of EEGs: nonstationarity, oscillatory patterns with essentially different types of oscillations (which implies an adaptive approach to the study of various effects on EEGs), and the high noise level. Moreover, the analysis of short-term time series data is frequently needed, as dictated by both data recording conditions and the specific features of brain processes [113, 122–124].

The apparatus of wavelet analysis is successfully being applied to studying normal and pathological EEGs of animals and humans [20, 125–128]. The attention of researchers was focused on an analysis of the development of specific forms of rhythmic activity associated with such functional states as episodes of epileptic activity, sleep, and wakefulness. As known, the presence of rhythmic components in EEGs reflects synchronous activity of the huge number of nerve cells arranged in assemblies [129–131]. Therefore, the study of rhythmic activity in cerebral EEG dynamics is closely related to such problems of importance for radiophysics and nonlinear dynamics as the investigation of the synchronous behavior in networks with intricate topological connections [106–108, 132].

5.1 Automated extraction of spike-wave discharges on prerecorded EEGs

Pathological processes in the CNS may be associated with an enhanced degree of synchronization among functionally connected structures. In extreme cases, it can lead to the appearance of paroxysmal discharges on EEGs. For example, absence epilepsy (see below) develops against the background of hypersynchronized neuronal activity in the thalamocortical network [133, 134]. The interaction processes in the thalamocortical network associated with the initiation of absence epilepsy are convenient to study in selectively bred rat lines genetically predisposed to this form of the disease, e.g., WAG/Rij [135]. Epileptic seizures in these animals (similarly to humans) are accompanied by high-amplitude hypersynchronous spike-wave activity apparent on EEGs (spike-wave discharges).

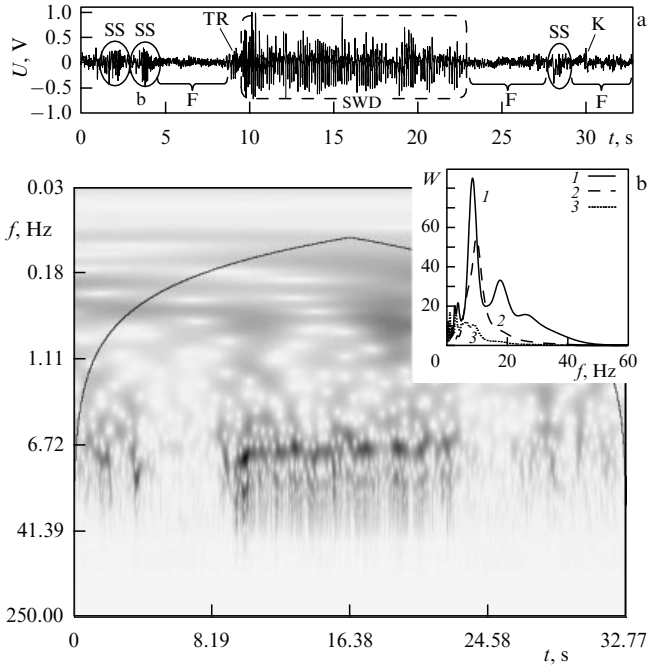

Figure 17. A portion of an epileptic EEG (a) and the corresponding wavelet spectrum constructed with the use of the Morlet wavelet basis (b). Distinguished regions: SWD — spike-wave discharge, SS — sleep spindle, TR — theta-activity episode, K — K-complex, and F — normal brain background activity. The inset shows instantaneous oscillation wavelet spectra: spike-wave discharge (*1*), sleep spindle (*2*), and background activity (*3*).

Let us consider a portion of an epileptic EEG taken from a WAG/Rij rat (Fig. 17a). The brain electrical activity was recorded in conscious rats having electrodes implanted in the frontal cortex. A few components differing in oscillation shape and amplitude can be distinguished in the EEG signal.[6] For example, background dynamics corresponding to the desynchronized behavior of neural assemblies in cerebral cortex is characterized by a small amplitude (F regions in Fig. 17a). Oscillatory patterns can be classified by shape and frequency composition. The first method is traditionally used in neurophysiology [136, 137] to discriminate between such oscillatory patterns as sleep spindles (SS regions in Fig. 17a), bursts of theta-activity (TR), K-complexes (K), and spike-wave discharges (SWD). The second method provides a more precise tool for the analysis of time series and may be applied for automated recognition of structures in the time domain. The results of continuous wavelet analysis using the Morlet wavelet are presented in Fig. 17b showing that various EEG patterns correspond to different frequency distributions of energy. Specifically, a spike-wave discharge (an epileptic event on EEGs) possesses two important features.

First, analysis of a large number of spike-wave discharges showed [128] that the main spike repetition frequency

[6] In what follows, different EEG fragments will be referred to as oscillatory patterns.

decreases smoothly during the discharge from the maximum value at the beginning (11.1 ± 1.5 Hz; here and hereinafter, $\pm$ denotes standard deviation) to 7.4 ± 0.8 Hz at the end, i.e., by 2.8 ± 0.8 Hz on the average. Second, the appearance of epileptic (spike-wave) discharges on EEGs was associated with a sharp power rise within a frequency range from 10 to 100 Hz, with each individual spike entering into the spike-wave complex being represented in the wavelet spectrum by a local power burst (see inset to Fig. 17b). These high-frequency spectral components generated by the regular spike sequence on EEGs were important diagnostic signs that provided a basis for the development of an algorithm for automated recognition of spike-wave discharges [62, 138, 139].

Since a spike-wave discharge is characterized by a rise in the energy per certain scale range, it is convenient to consider the integral instantaneous energy in some frequency range:

$$w_{F_S}(t) = \int_{F_S} \left|W(t, f)\right|^2 \mathrm{d}f, \tag{28}$$

where $F_S = [30, 50]$ Hz is the frequency range in which structural differences between spike-wave discharges and other oscillatory patterns are especially apparent. If a spike-wave discharge occurs at a certain time moment t, the following relation holds:

$$w_{F_S}(t) \geqslant E_k\,, \tag{29}$$

where E_k is the threshold energy value determined experimentally. We used threshold sorting for automated diagnostics of epileptic events.

Moments of time at which the value of w_{F_S} (29) exceeded the threshold level and did not decrease within the next 1 s were regarded as marking the onset of epileptic activity, and those when the energy level dropped below the threshold as the end of discharges. The results of automated extraction of spike-wave discharges are presented in Table 3, where the following notations are used: TP — the number of rightly recognized events on the EEG, TN — the number of correctly detected absences of the event of interest (spike-wave discharge), FP — the number of misrecognized events (i.e., the number of events identified as spike-wave discharges by the automated EEG marking system but as some other type of activity by the expert), and FN — the number of missed spike-wave discharges. The accuracy of recognition of spike-wave discharges on EEGs by this method amounted to 98–100%. It should be emphasized that spike-wave discharges were distinguished by analyzing similar frequency ranges $F_S = F_{SWD} \in [30, 50]$ Hz (28) and threshold energy values $E_k = 0.5$ (29) in wavelet spectra.

In the qualitative analysis of algorithm performance, the statistical characteristics of taking the 'binary' solution were applied (presence/absence of an epileptic event) based on a criterion that with a certain degree of probability could lead to a false result: the confidence level $\beta = (\mathrm{TP}/(\mathrm{TP} + \mathrm{FN}))\,100\%$, and the power of a test $\delta = (\mathrm{TN}/(\mathrm{TN} + \mathrm{FP}))\,100\%$ [140]. The values of β and δ are also presented in Table 3 for each animal. The former characteristic (β) allows an estimation of sensitivity of the method, i.e., the percentage of recognized spike-wave discharges out of their total number on the EEG. The latter characteristic (δ) permits estimating percentage of events correctly identified as spike-wave discharges out of the total number of events diagnosed as spike-wave discharges [62, 141]. These findings showed that the method for recognition and identification of EEG oscillatory patterns based on the wavelet transform significantly surpasses other available methods in terms of accuracy, simplicity of tuning, and adaptation to the solution of other problems.

The most important results of continuous wavelet analysis of spike-wave discharges include the unique features of the time-frequency EEG structure observed before the onset of the epileptic discharge; they can be utilized to predict the development of epileptiform activity. Our study with the use of the complex Morlet wavelet showed that the appearance of spike-wave discharges on EEGs is preceded by a totality of short rhythmic components with a maximum power in the delta (3–5 Hz) and theta/alpha (7–11 Hz) frequency ranges [128]. Low-frequency delta and theta/alpha components preceded 90% and 92% of the spike-wave discharges, respectively. The mean duration of the precursors was roughly half a second. Only 5% of the spike-wave discharges had no rhythmic precursors on the EEGs. Both components (delta and theta/alpha) were simultaneously present on the EEGs prior to spike-wave discharges only in 89% of the events. Such a situation is not typical of baseline EEGs. A more detailed discussion of neural mechanisms underlying the formation of predecessors of epileptiform activity can be found in our work [128]. It should be emphasized that these precursor complexes appearing before spike-wave discharges could be recognized only by time-frequency EEG wavelet analysis.

5.2 Structure and automated isolation of sleep spindles on epileptic EEGs with the use of complex adaptive wavelet bases

Extensive neurophysiological studies are currently underway to elucidate the relationship between spike-wave discharges and normal brain synchronous activity (sleep spindles) [109, 142, 143] apparent on EEGs in the second sleep phase (S-sleep) in the form of characteristic spindle-

Table 3. Results of automated extraction of spike-wave discharges (SWDs) with the use of the complex Morlet wavelet ($f_0 = 1$).

Rat No.	Number of SWDs (expert visual assessment)	Automated extraction				Quality of automated marking		
		TP	TN	FP	FN	Accuracy ρ_{SWD}, %	Significance level β, %	Power of a test δ, %
1	105	105	105	0	0	100.0	100.0	100.0
2	81	79	80	2	1	97.5	98.8	97.5
3	249	247	250	1	2	99.2	99.2	99.6
4	120	117	125	1	3	97.5	97.5	99.2
5	66	65	67	2	1	98.5	98.5	97.0
Mean						98.5 ± 1.1	98.8 ± 0.9	98.7 ± 1.3

shaped oscillations with a frequency of 10–15 Hz and of 0.5–1.5 s duration with the amplitude initially increasing and thereafter decreasing. Sleep spindles are regarded as resulting from the synchronous dynamics of neural networks under normal conditions. They attracted the attention of researchers after the publication of experimental data on the transformation of sleep spindles into epileptic spike-wave discharges [144, 145].

The structure of sleep spindles on EEGs was studied during slow-wave sleep in WAG/Rij rats with the help of continuous wavelet transform using the complex Morlet wavelet. Figure 18 shows a characteristic sleep EEG wavelet spectrum with extracted spindles, and the corresponding sleep spindle spectra in the alpha range (from 8 to 14 Hz). Unlike spike-wave discharges, the spindles differed in shape and frequency composition [62], which strongly hampered their identification and automated recognition. For threshold detection of wavelet power [see formulas (28) and (29)] in the 8–14 Hz frequency range (see Section 5.1), the accuracy of recognition of sleep spindles on EEGs did not exceed 60% at a low confidence level and strength of test. Therefore, a novel approach to the study of the structure of nonstationary signals was developed based on adaptive wavelet analysis [62, 146]. The latter uses an arbitrary EEG fragment showing maximum affinity to the sought EEG pattern as the 'mother' function and serves as a tool for the recognition and localization of oscillations having a nonstandard intricate shape on EEGs. This approach is, in fact, a variant of the known template matching method [147] and thus can be applied to effectively extract sleep spindles, standardize the EEG structure, and create a reference base of EEG patterns.

Special wavelet bases (spindle wavelets [62, 146]) were constructed from EEG oscillatory patterns containing sleep spindles to standardize their structure; in other words, spindles present on real EEGs served as templates for the construction of a mother spindle wavelet (see Fig. 19 clearly illustrating the proposed method).

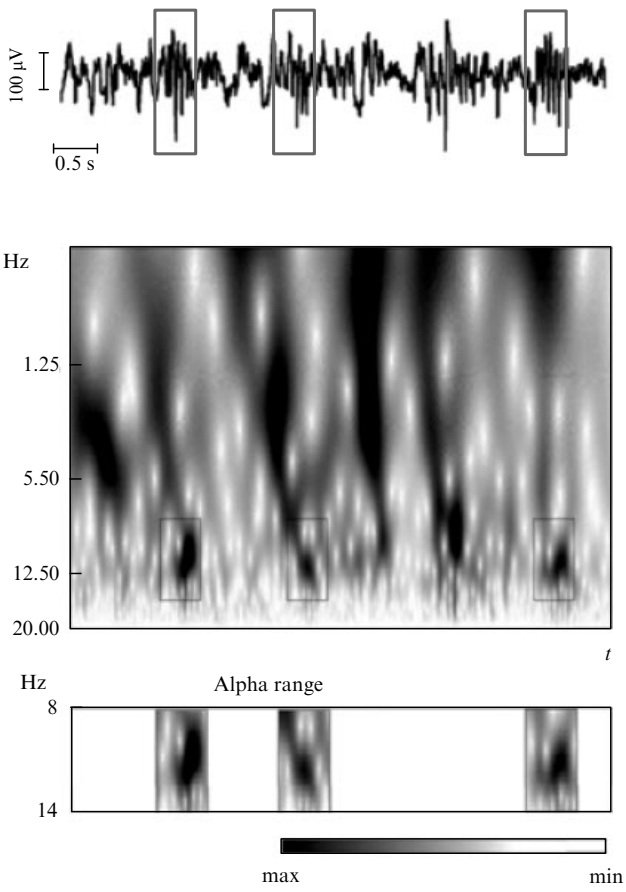

Figure 18. Continuous wavelet transform with the complex Morlet wavelet of sleep spindles (rectangles on the EEG). Bottom: portion of the wavelet spectrum in the alpha range (8–14 Hz).

Let us formalize this approach. Let $U(t)$ be a fragment of the recorded EEG signal containing a sleep spindle. Let us

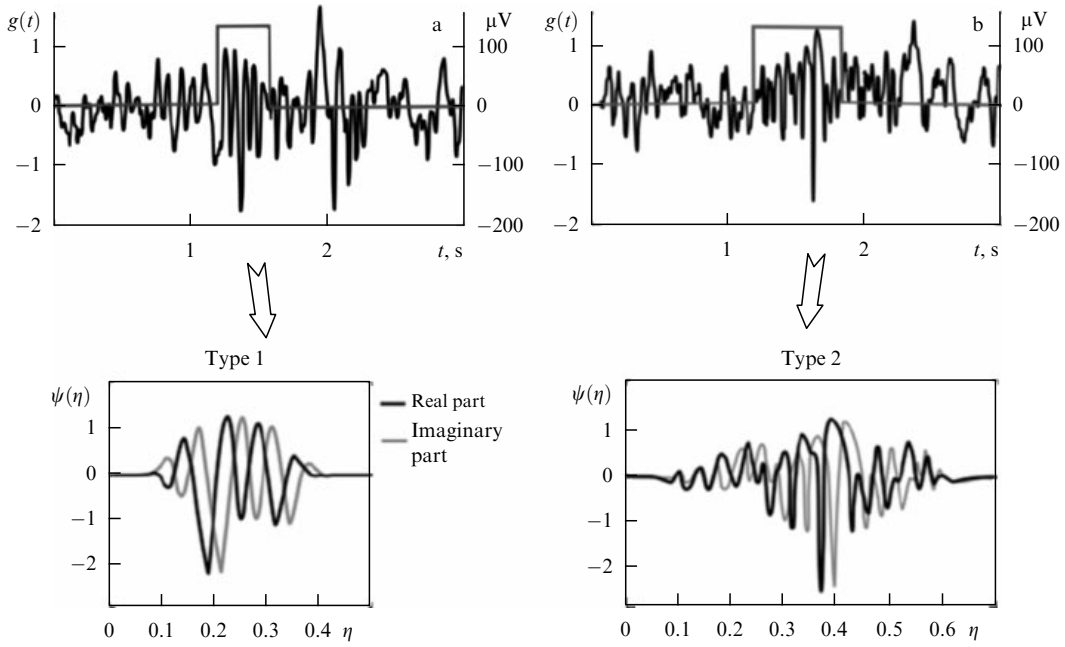

Figure 19. Diagrams illustrating construction of 'spindle' wavelets. Prototype sleep spindles selected on EEGs are used as templates for adaptive wavelet bases: type 1 (a) and type 2 (b) spindle wavelets.

Table 4. Results of automated extraction of sleep spindles with the use of spindle wavelets. Here, N_{S1} is the number of spindles missed in automated extraction with the use of a type 1 spindle wavelet.

Type 1 spindle wavelet

Rat No.	Number of sleep spindles (expert visual assessment)	Automated extraction			Quality of automated marking		
		TP	FP	FN	Accuracy ρ_S, %	Significance level β, %	Power of a test δ, %
1	2341	2130	23	281	91.1	88.4	98.9
2	1381	1132	28	110	82.2	91.2	97.6
3	1491	1312	30	149	87.8	89.8	97.8
4	1305	1096	39	104	83.9	91.3	96.6
5	1598	1422	16	144	88.9	90.8	98.9
Mean	1623 ± 416	1418 ± 419	27 ± 9	157 ± 72	86.8 ± 3.7	90.3 ± 1.2	97.9 ± 1.0

Type 2 spindle wavelet

Rat No.	N_{S1}	Automated extraction				Quality of automated marking		
		TP	TN	FP	FN	ρ_S, %	β, %	δ, %
1	211	140	2154	70	22	66.3	96.9	86.4
2	249	110	1215	69	21	44.2	94.6	84.0
3	179	164	1327	30	15	91.6	97.8	91.6
4	209	117	1175	26	18	56.0	97.8	86.7
5	176	112	1454	48	14	63.6	96.8	88.9
Mean	205 ± 30	129 ± 23	1465 ± 400	48.6 ± 20.8	18 ± 6	64.3 ± 17.5	96.8 ± 1.3	87.5 ± 2.9

further move to a signal with an excluded middle:

$$g(t) = U(t) - \frac{1}{\Delta T}\int_{\Delta T} U(t)\,\mathrm{d}t\,, \tag{30}$$

and build up the complex function

$$\hat{g}(\eta) = g(\eta) + \mathrm{i}g\left(\eta + \frac{T}{4}\right), \tag{31}$$

where T is the characteristic oscillation timescale during the spindle occurrence. In order to obtain the local-in-time wavelet basis, function (31) is modulated with the Gaussian function [cf. relation (1)]

$$\psi^{S}(\eta) = A\hat{g}(\eta)\exp\left(-\frac{\eta^2}{\alpha}\right), \tag{32}$$

where α is the fitted coefficient, and parameter A is found from the normalization condition

$$A^2\int_{-\infty}^{\infty}\left|\hat{g}\left(\frac{2\eta}{\alpha}\right)\right|^2\exp\left(-\eta^2\right)\mathrm{d}\eta = 1\,. \tag{33}$$

Roughly a total of 100 spindles were tested as templates for the spindle wavelet, and each spindle was used to analyze the results of the extraction of sleep spindles. As a result, the universal spindle wavelet shown in Fig. 19a was found to ensure the best quality of recognition of sleep spindles and show, accordingly, a high affinity to the maximum number of sleep spindles on EEGs from all experimental animals. Most sleep spindles (80–90% in different experiments) had high affinity to the wavelet basis employed (they were called type 1 spindles). Their shape bore a close resemblance to the sinusoidal shape and the frequency varied from 8 to 12 Hz. The remaining spindles (roughly 10–15% of the total) had an intricate shape and specific individual features (type 2 spindles, see Fig. 19b). That is why new mother wavelets had to be constructed for their identification, with EEG patterns assorted for each concrete animal). The wavelet bases of type 2 spindles had a nonuniform shape with apparent irregular spikes; their frequency on EEGs varied from 17 to 23 Hz.

The results of automated extraction of type 1 and 2 sleep spindles are presented separately in Table 4. All notations are analogous to those in Table 3. Clearly, the approach based on the construction of adaptive bases allowed substantial improvement of the quality of recognition of the patterns in the nonstationary EEG signal.

To recall, the percentage of recognized sleep spindles with the use of the standard Morlet wavelet as the basis function was rather small (less than 60%). Combined application of wavelet bases of type 1 and 2 spindles permitted automatically recognizing 96–100% of the sleep spindles present on the EEG (much more than by other methods).

Application of wavelet methods for the automated analysis and diagnostics of oscillatory patterns (sleep spindles and spike-wave discharges) made it possible to elucidate the dynamic regularities in their appearance from long-term (24 hour) EEG recordings [138, 145, 148]. It was revealed, in particular, that the dynamics of spike-wave discharges and sleep spindles determined by synchronous dynamics of the cortical neural network exhibits the on–off intermittent behavior [149, 150] usually observed at the boundary of synchronous oscillatory modes of coupled chaotic oscillators [151–154]. These findings led to important inferences about common mechanisms of the generation of sleep spindles and spike-wave discharges in the brain's thalamocortical network and possible transformation of sleep spindles into epileptic events [121, 145]. Such studies would be impossible without automated methods for the diagnostics of oscillatory patterns, bearing in mind large amounts of experimental data for the elucidation and analysis of relevant statistical regularities.

5.3 Classification of oscillatory patterns appearing on EEGs with the use of adaptive wavelet bases

As shown in Section 5.2, it is possible to construct different types of adaptive wavelet bases for the optimal description of

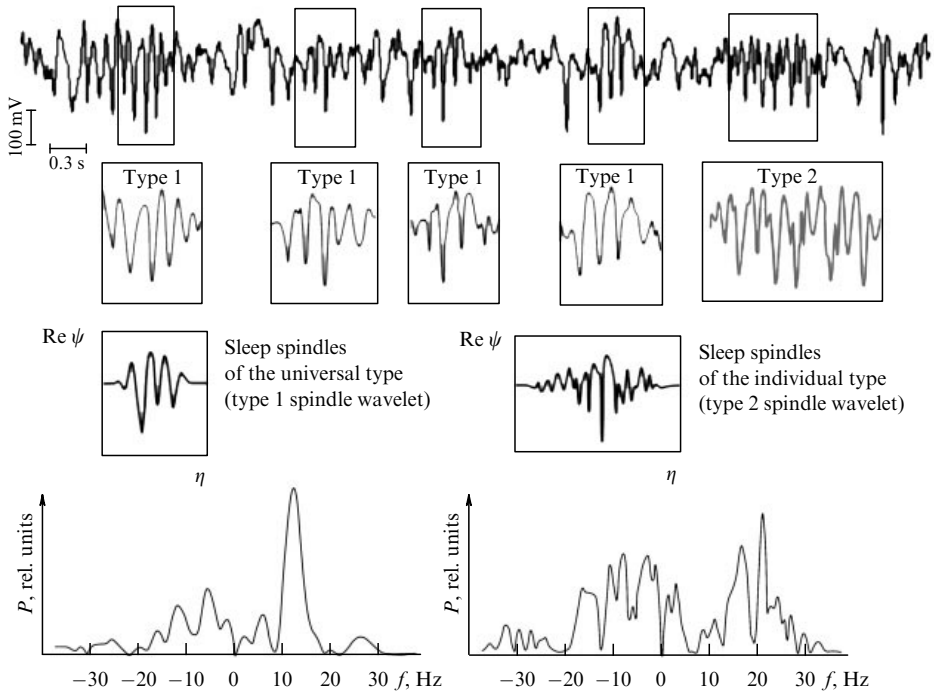

Figure 20. Shape variability of sleep spindles on the EEGs of WAG/Rij rats. Most spindles are extracted using type 1 spindle wavelets universally applicable to all animal species. This type of oscillatory activity is regarded as a typical normal sleep spindle. However, the adaptive wavelet fails to identify some 10–15% of the spindles; individual wavelet bases for each rat need to be constructed to recognize them. Type 2 spindle wavelets have a more intricate shape unique for each animal. This type of oscillatory activity is associated with proepileptic activity on EEGs. The bottom of the figure displays Fourier spectra of type 1 and 2 spindle wavelets (left and right, respectively).

the structure of EGG oscillatory patterns (as exemplified by sleep spindles). Two types of sleep spindles differing in shape, frequency, and time of onset were distinguished on the EEGs of WAG/Rij rats.

Type 1 sleep spindles (typical ones) and spike-wave discharges contained a strong rhythmic component in the alpha-frequency range (corresponding to the 9–12 Hz frequency range in the Fourier power spectrum [62]). The power spectrum of spike-wave discharges was characterized by a narrow local maximum at 9.8 Hz, with the amplitude much in excess of the remaining part of the spectrum. This suggests that discharges had a regular periodic structure, while the oscillation period increased from the beginning to the end of the spike-wave discharge. The frequency of sleep-spindle activity significantly changed in the alpha range, as evidenced by the wide power spectrum pedestal in the respective frequency region. These spindles were typical normal spindles that accounted for over 85% of all observed sleep spindles on the epileptic EEG. The maximum of the oscillatory energy of these spindles occurred in the alpha range. The typical shape of type 1 spindles is illustrated in Fig. 20 (left). It follows from the Fourier spectrum of the type 1 spindle wavelet that the main energy is concentrated in the 8–14 Hz range.

Type 2 sleep spindles have a unique shape and characteristics for each experimental animal; they are extracted by continuous wavelet transform with the complex type 2 spindle wavelet (Fig. 20, right). This type is considered to be an intermediate form between sleep spindles and pathological spike-wave discharges [62]. The number of such events on an epileptic EEG does not, on average, exceed 10–15% of the total number of observed sleep spindles. A specific feature of these 'proepileptic' EEG patterns is the presence of intense peaks in both 4–8 Hz and 16–25 Hz regions of the power spectrum. Typical normal spindles do not produce such peaks.

5.4 Real-time diagnostics of oscillatory pattern origin on an epileptic EEG

Of primary importance today is the development of methods for real-time diagnostics of oscillatory patterns. The solution to this problem is of interest for designing brain activity monitoring systems in medicine [141, 155] and efficacious methods to be employed for creating specific brain–computer interfaces in the future [117–120]. Real-time diagnostics of oscillatory patterns is hampered by the similar spectral composition of topologically different patterns (i.e., structures belonging to different classes). For this reason, any method devised for recognizing such structures must, on the one hand, distinguish between patterns of similar frequency composition and energy and, on the other hand, ensure quite efficacious numerical realization for the construction of an actually operating system. Another difficulty for the real-time extraction of oscillatory patterns is the impossibility at the present moment of complete time-dependent realization needed for implementing transformation (3). Taken together, these make the development of a universal method for real-time diagnostics of oscillatory patterns both very interesting and difficult. We therefore will confine ourselves to the brief description of the currently accepted approach to real-time diagnostics of spike-wave discharges [141, 155].

The first problem touched upon in the foregoing can be resolved by applying the wavelet transform based on the complex Morlet wavelet selectively separating similar patterns. The second problem relates to a limited time series when the researcher has to deal with discrete signal amplitude values obtained starting from the onset of the experiment till a

Table 5. Results of real-time detection of epileptic patterns.

Rat No.	Number of events (expert visual assessment)	Automated extraction			Quality of automated marking	
		TP	FP	FN	Significance level β, %	Power of a test δ, %
1	101	101	3	0	100	97.1
2	29	29	0	0	100	100
3	43	43	2	0	100	95.6
4	66	66	1	0	100	98.5
5	44	44	2	0	100	95.7
6	66	66	4	0	100	94.3
7	115	115	3	0	100	97.5
8	56	58	2	0	100	96.6
Mean	65 ± 29	65 ± 29	2.1 ± 1.3	0.0 ± 0.0	100 ± 0	96.9 ± 1.8

given moment. This problem can be resolved taking into account the fact that wavelet function (2) rapidly decreases with time, i.e., the largest part of the power is concentrated within a certain time interval; then, expression (1) can be substituted by the following one, practically without the loss of accuracy:

$$W(a,b) \approx \int_{b-\Delta T}^{b+\Delta T} x(t)\,\psi^*\left(\frac{t-b}{a}\right) \mathrm{d}t\,. \tag{34}$$

This means that a part of the realization $2\Delta T$ in duration is needed in order to calculate the energy per certain scale at a given instant of time. Importantly, whether a spike-wave discharge occurred at the moment of time t can be determined only at moment $t+\Delta T$. Thus, quantity ΔT is an essentially unavoidable delay of automated diagnostics. This quantity is determined by the type of the mother wavelet and the time scale a for which the transformation is performed. For the Morlet mother wavelet, one finds $\Delta T \approx 4a$, where a is the time scale of interest.

Let us consider some peculiarities of the realization of the real-time diagnostic algorithm for oscillatory patterns on EEGs [141, 155]. The method is based on the computation of the wavelet spectrum (34) and the wavelet transform energy (28) per scale range F_S at each instant of time. The rectangle method was applied for numerical integration when computing the instantaneous wavelet transform energy (28). We considered 15 time scales proportional to 15 frequencies uniformly distributed over the above range. It was shown that the use of 15 scales leads to a sensible compromise between the accuracy of calculation of the wavelet spectrum and computational speed. It should be noted that an EEG may exhibit isolated bursts of high-frequency activity during the normal (nonepileptic) period, e.g., K-complexes [106]. Such events may lead to a sharp rise in the instantaneous transformation energy and erroneous detection of the epileptic pattern. Because such energy bursts occurred rather frequently, the algorithm described in Section 5.1 was modified to improve the accuracy and reliability of analysis. For example, we diagnosed the type of oscillations in formula (29) based on the threshold value of E_k as the criterion taking not the instantaneous value of the transformation energy (28) but the value averaged over a certain time interval:

$$\langle w(t)\rangle = \frac{1}{K_0}\int_{K_0} w(t)\,\mathrm{d}t\,. \tag{35}$$

In such a case, the greater the window size K_0 over which averaging is performed, the higher the accuracy of the diagnostic method, and yet the greater the time needed to detect a discharge. The following algorithm was developed for automated diagnostics of a definite type of oscillatory activity on EEGs with the use of the wavelet transform: at each instant of discrete time determined by the discretization frequency of the data collection system, wavelet transformation is performed for all scales within the specified range, instantaneous (28) and averaged (35) wavelet energies in the scale range are calculated, following which condition (29) is checked. The high reliability of the method is achieved by individually choosing the threshold value of energy E_k from an EEG section one hour in duration for each object being analyzed. Usually, E_k is 2.5–3 times the average energy value in the same frequency range in the absence of a spike-wave discharge.

This method was utilized to create a system for real-time diagnostics of epileptic discharges based on the WinDAQ data acquisition system.[7] The system was employed to realize bidirectional data exchange with ADC/DAC units. As soon as the system detected a spike-wave discharge, it sent a rectangular pulse to a DAC input that could be used both to record the discharge and to control the operation of an external device, e.g., an electronic generator acting on the brain of an experimental animal. The resulting feedback proved instrumental in substantially extending the possibilities of using the diagnostic system in experimental studies. Specifically, it allowed the application of external factors to prevent (eliminate) the development of hypersynchronous activity (epileptic discharge) in the cerebral cortex.

The results of experimental verification of the method on EEG 5-h recordings are presented in Table 5. It demonstrates the highest confidence level β amounting to 100%, mean power of a test $\delta = 96.9\%$, and mean time delay needed to recognize a spike-wave discharge covered 1.00 ± 0.55 s after the onset of the event. The last parameter depended in the first place on the window size over which averaging was performed, and could be significantly decreased or increased because the time of performing transformation at the discretization frequency employed (500 Hz) was much shorter than the time between two consecutive countings.

The efficacy of the method was estimated in a 24-h-long experiment (EEG recording). The real-time performance of the automated recognition system is illustrated in Fig. 21. It can be seen that the number of erroneously detected and unrecognized events slightly changed with time due to minor alterations in the shape of spike-wave discharges in different

[7] See http://www.dataq.com/.

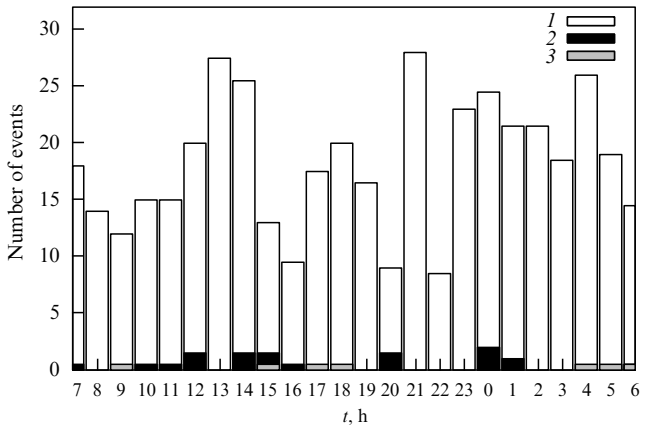

Figure 21. Time distribution of events during a 24-hour experiment: *1* — rightly recognized spike-wave discharges, *2* — misrecognized events erroneously identified as spike-wave discharges, and *3* — missed spike-wave discharges.

phases of the sleep/wakefulness cycle. On the whole, this number remained small during the entire experiment.

5.5 Artifact suppression by combining wavelets and independent component analysis

Standard methods of signal structure analysis (e.g., classical spectral analysis) are not always directly applicable to EEG studies due to artifacts in the experimental data. The amplitude of these artifacts, induced by eye movements, winking, muscular activity, etc, may be much greater than that of the brain electrical activity of interest for the researcher. At present, a visual (or semiautomatic) method for the recognition of artifacts is employed, and frequently they are removed manually. Usually, oscillatory patterns (EEG sections) containing an artifact are cut out of the long recording. This procedure is highly subjective and requires great caution on the part of the experimentalist; not infrequently, it significantly reduces the amount of experimental data for further analysis. For example, only a 1-min long 'pure' fragment is sometimes available out of the 10-min EEG recording from a healthy human. In medical practice, the loss of experimental data may be even greater, e.g., in the analysis of EEGs of children [156] or patients with certain diseases [157]. It substantially lowers the efficacy of diagnostic studies. A reduced sample size along with segmentation of experimental data (integration of artifact-free oscillatory patterns) poses a number of questions related to the stationarity of the process composed of integrated pieces; hence, the attractiveness of establishing procedures for the deletion of artifacts other than excision of EEG sections.

An EEG record from a single electrode can be regarded as a mixture of signals from different brain regions and artifacts. In the first approximation, neural signals and artifacts may be regarded as independent processes [158, 159]. An efficacious method has recently been proposed to suppress artifacts based on independent component analysis (ICA) [160]. It was modified in later studies [161–163]. The use of ICA is actually an attempt to separate a recorded EEG signal into statistically independent components for the elimination of those responsible for artifacts. ICA was most frequently applied to the analysis of EEGs for the efficacious removal of visual artifacts [161–165]. Currently, ICA is considered to be a promising tool for the 'purification' of EEG signals. A few remarks are in order in this context.

(1) Identification of components responsible for artifacts depends on preliminary knowledge of their structure and the experimentalist skills. Moreover, short oscillatory patterns ($\sim$ 10 s) need to be used for efficacious performance of the algorithm [166].

(2) Despite the known efficacy of ICA as a tool for artifact elimination from EEGs, there are few quantitative data demonstrating its advantages and disadvantages. By way of example, it was argued in Refs [156, 165] that ICA may lead to distortions in the power spectrum of the brain's electrical activity proper.

Worthy of note are numerous examples of wavelet application to EEG analysis [167–172]. It was shown in a recent study [173] that the preliminary wavelet-based purification of an EEG from noise may increase the efficacy of subsequent ICA. A tighter integration of ICA and wavelet transform analysis might yield even more interesting results.

One of the authors of the present review proposed a new approach — wavelet analysis of independent components (WAIC) [174]. This method is based on ICA and implies the employment of wavelets as an intermediate stage of the integrated artifact suppression algorithm, instead of preliminary filtering of experimental data.

ICA approach is based on three main assumptions:

(1) experimental data are a mixture of independent processes of neuronal activity and artifacts;

(2) superposition of electric potentials from different brain regions near the electrode is linear, and the signal propagation time from the source to the electrode is negligibly small;

(3) the total number of sources of activity (both neuronal and artifactual) does not exceed the number of electrodes.

Thus, number K of simultaneously recorded EEG signals $X(t) = (x_1(t), \ldots, x_K(t))^{\mathrm{T}}$ is a linear combination N ($N \leqslant K$) of the initially unknown components (sources) $S(t) = (s_1(t), \ldots, s_N(t))^{\mathrm{T}}$ describing the processes of neuronal activity and artifacts:

$$X(t) = MS(t)\,, \tag{36}$$

where M is the matrix with unknown elements determining the weighted contribution of each source to the recorded EEG signal. The purpose of ICA is to find $S(t)$ and M directly from $X(t)$. The numerical algorithm for ICA was proposed, in particular, in Ref. [160] and modified later in Refs [175, 176]. It makes use of neural networks maximizing joint entropy and minimizing mutual information from output components of the neural processor. Other variants of ICA realization can be used for the purpose of control [177].

The artifact suppression algorithm was tested by standard EEG recording in healthy humans with open eyes [178]. The application of ICA allowed analyzing the temporal structure $S(t)$ and topography M of EEG signal components. For example, winking-induced visual artifacts largely affected signals from frontal electrodes; they were accompanied by a strong burst roughly 1 s in duration (Fig. 22a). It was proposed in Ref. [160] that artifact-containing components be set to zero when forming a new matrix $\hat{S}(t)$. For example, if the first component contains artifacts, then $\hat{S}(t) = (0, s_2(t), \ldots, s_N(t))^{\mathrm{T}}$. EEG signals purified by ICA were reconstructed after removal of the artifact sources:

$$\hat{X}(t) = M\hat{S}(t)\,. \tag{37}$$

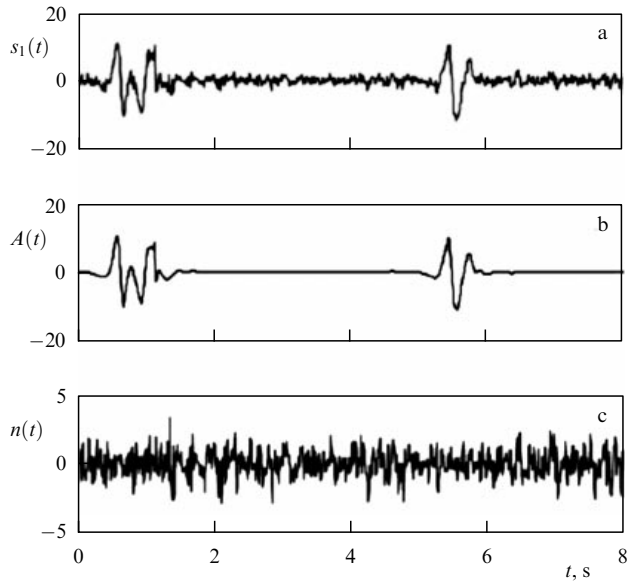

Figure 22. Expansion of an independent component into two constituents representing artifacts and neural activity, respectively [see Eqn (38)]: (a) independent component $s_1(t)$ extracted by ICA and showing two winking episodes (around 0.8 s and 5.5 s); (b) artifactual component $A(t)$, and (c) neuronal activity $n(t)$.

Let us see how the utilization of wavelets permits improving the efficacy of artifact suppression. Independent components of EEG signals containing artifact sources may also include the contribution from neuronal activity by virtue of the limitation on the maximum number of independent sources or other causes [166]. The removal of such components results in the loss of part of the neuronal activity and, therefore, in distorted EEG representation [179]. Figure 22 illustrates such a situation (the first independent component $s_1(t)$ contains two winking-driven artifacts). This component cannot *a priori* involve other artifacts unrelated to those induced by eye movements. It can be divided into a high-amplitude artifact $A(t)$ (Fig. 22b) and a low-amplitude neural signal $n(t)$ (Fig. 22c):

$$s_1(t) = A(t) + n(t)\,. \tag{38}$$

We note that the artifact disappears outside the winking segments (Fig. 22b), but the original component $s_1(t)$ contains an appreciable contribution from the neural signal.

In the framework of the standard method, component $s_1(t)$ is equated to zero prior to the reconstruction of a purified EEG signal, with the loss of part of the neuronal activity:

$$\hat{x}_j(t) = r_j(t) - m_{j1}n(t)\,, \tag{39}$$

where $r_j(t) = x_j(t) - m_{j1}A(t)$ is the signal with the removed artifact, and m_{j1} is the corresponding weight coefficient of matrix M.

Could we extract the neural component of signal $n(t)$ from $s_1(t)$, it would enable us to correct the reconstruction of the filtered EEG recording. The expansion of the independent component $s_1(t)$ into two constituents (38) is initially unknown, but they can be found from the properties of signals $A(t)$ and $n(t)$. Thus, the high-power artifact $A(t)$ is localized in time and frequency, while signal $n(t)$ has a low amplitude and wider spectrum (see Fig. 22). These features of the signals make possible their separation in the time–frequency spectrum of the wavelet transform.

The first independent component $s_1(t)$ being the sum of two terms (38), its wavelet transform is also expressed in the form of a sum:

$$W_s(a,b) = W_A(a,b) + W_n(a,b)\,, \tag{40}$$

where $W_A(a,b)$ and $W_n(a,b)$ are the wavelet transform coefficients of signals $A(t)$ and $n(t)$, respectively. As noted above, the artifactual dynamics are characterized by relatively large coefficient values and localization in the time–frequency region, whereas the neuronal dynamics are manifested in a broader scale range and with a much lower energy. This is clearly seen in Fig. 23 presenting the results of wavelet transformation of the three signals depicted in Fig. 22. Sections of wavelet spectra dominated by artifact-related high-amplitude dynamics are apparent. These segments are short and localized in the large scale region. The neuronal dynamics are characterized by a more uniform distribution of coefficients that have rather small values. Due to this, artifacts can be removed by introducing a filtration threshold beyond which suprathreshold wavelet coefficients describing them are set to zero; thereafter, inverse wavelet transform is accomplished. It should be noted that this procedure is much easier (and faster) to perform for DWT; however, the use of CWT gives better results. The procedure for the extraction of neuronal activity is very similar to wavelet-based noise filtration [180], but it has an opposite purpose, namely, to separate a weak broad-band meaningful signal from artifacts with higher energies.

WAIC proposed for artifact suppression in EEGs implies the following sequence of actions:

(1) Application of the standard variant of ICA to the treatment of experimental EEG recordings, derivation of the weight matrix M and time-dependent dynamics of independent components $(s_1(t), s_2(t), \ldots, s_N(t))^{\mathrm{T}}$.

(2) Direct wavelet transform of components $\{s_i(t)\}$ to obtain coefficients $\{W(a,b)\}_i$.

(3) Empirical introduction of the threshold value of W^* and setting to zero coefficients exceeding the specified threshold level: $W(a,b) = 0$, if $|W(a,b)| > W^*$.

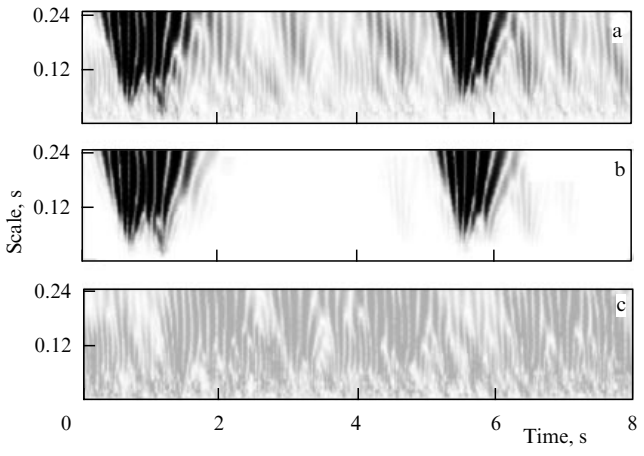

Figure 23. Results of wavelet transformation of independent component $s_1(t)$ (a), and its artifactual (b) and neuronal activity (c) constituents (based on the data shown in Fig. 22).

(4) Inverse wavelet transform to obtain adjusted components reflecting only neural dynamics $\{n_i(t)\}$.

(5) Extraction of the corrected EEG signal: $X^*(t) = M(n_1(t), \ldots, n_N(t))^{\mathrm{T}}$.

The choice of the suitable threshold value of W^* is of importance in the framework of the present algorithm. Approaches to the choice are discussed in Ref. [181] and its recommendations can be effectively applied in practical work to adjust the algorithm for the improvement of artifact suppression. The proposed algorithm allows overall automation and does not require 'manual' identification of artifacts.

WAIC applications for the suppression of winking and heartbeat artifacts are illustrated in Ref. [174]. Artifacts of the former type are seen on EEGs as large-amplitude impulses well localized in time. Those of the latter type emerge when the electrode resides close to an artery (the appropriate noise has the form of short and relatively small-amplitude impulses with a frequency on the order of 1 Hz). It was shown that WAIC permits reducing distortions of the electrical potential by one order of magnitude. Also, it is associated with many fewer distortions of neural signals beyond the artifact-containing regions. Some additional advantages of a modified WAIC are discussed in Ref. [174].

5.6 Analysis of the formation of hypersynchronous brain states from multichannel EEG recordings in patients with absence epilepsy by wavelet transform

We would like to conclude this review by referring to one more novel option available for wavelet application to EEG processing. Different cerebral cortex regions are known to operate synchronously under both normal (e.g., cognitive activity) and pathological (Parkinson's disease, various forms of epilepsy) conditions [1, 112]. These synchronous states can be studied by wavelet analysis of multichannel EEG recordings from different brain regions. By way of example, we shall address the analysis of the evolvement of a hypersynchronous epileptic discharge on EEGs from patients with absence epilepsy, a quite common neurologic disorder associated with total or partial loss of consciousness. Absence seizures usually last from a few seconds to tens of seconds; they are accompanied by characteristic spike–wave complexes on EEGs [182]. Spike-wave discharges recorded during epileptic seizures have a high amplitude and frequency on the order of 3.0 Hz. As is known, absence seizures are associated with enhanced synchronization between spacious brain regions and the appearance of hypersynchronous spike-wave discharges on EEGs. The source of epileptic activity and synchronization dynamics during spike-wave discharges remain to be elucidated and raise concerns among researchers and clinicians [13, 183].

One of the promising applications of wavelets in this context is the diagnostics of synchronous activity in complicated multifrequency signals of different natures. The general principle of synchronization diagnostics using a continuous wavelet transform with a complex basis (time scale synchronization) was developed and tested in Refs [48, 64, 65, 184]. The concept of time scale synchronization (see papers [48, 64] for details of the method) is underlain by the dynamic analysis of phase difference families, $\varphi_{a1}(t)$ and $\varphi_{a2}(t)$, obtained by continuous wavelet transform [see formula (4)] with the 'mother' Morlet wavelet of signals $x_1(t)$ and $x_2(t)$. This approach reveals synchronization of the selected spectral component of signals from two sources on a time interval ΔT, provided the phase difference in this interval is limited by a certain constant:

$$\left|\varphi_{a1}(t) - \varphi_{a2}(t)\right| < \text{const}\,. \tag{41}$$

Because phase families $\varphi_{a1}(t)$ and $\varphi_{a2}(t)$ of the EEG signals of interest are introduced with the help of the wavelet transform, this method proves resistant to noises, the intricate shape and nonstationarity of the signal being analyzed. Thanks to these circumstances it provides the possibility of comprehensively describing peculiar features of temporal and spatial synchronization of electrical activity between different brain regions in normal and paroxysmal states.

Let us consider as an example the formation of a hypersynchronous state on an EEG during a seizure in a patient with severe absence epilepsy. The EEGs were recorded in a diagnostic clinic using the standard 10–20 system of electrode arrangement on the head [185]. Figure 24 shows the position of electrodes and a typical section of an EEG recording with a spike-wave discharge.

The source of spike-wave discharge was localized based on the study of pairwise time scale synchronization (41) between all EEG channels shown in Fig. 24. The dynamic analysis involved instantaneous phases in a narrow frequency range of 3–4 Hz, into which the largest fraction of

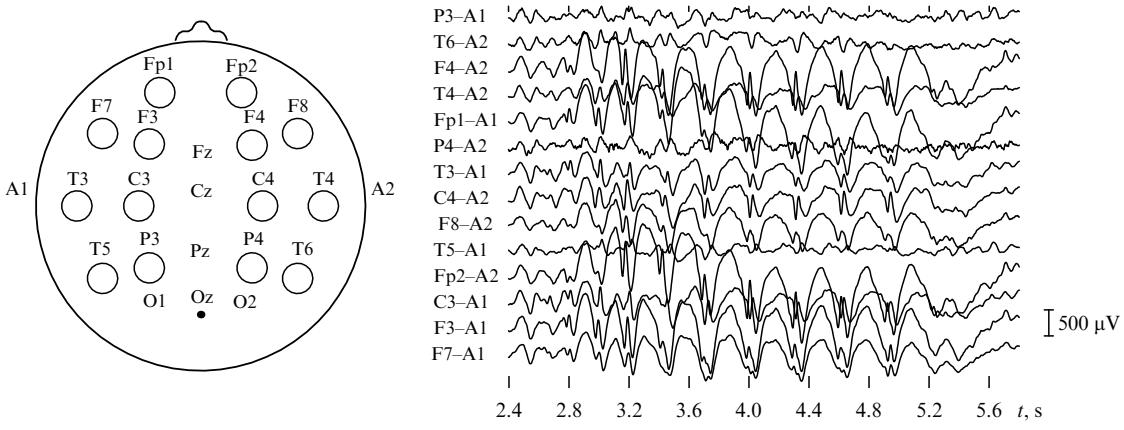

Figure 24. (a) Standard electrode arrangement on the patient's head (10–20 system). Signals from electrodes enclosed by circles were used in synchronization analysis. (b) An example of a typical multichannel EEG showing a spike-wave discharge.

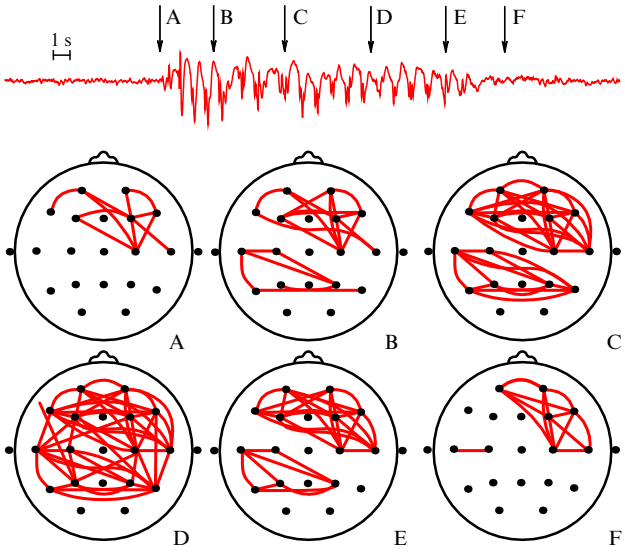

Figure 25. Dynamics of spike-wave discharge from the perspective of synchronization of different brain regions — the number of synchronized regions increases as the discharge develops; almost all cortical regions prove synchronized by the end of the event. Diagrams correspond to different instants of time indicated by arrows A – D on the bipolar EEG recording from the frontal region (electrodes F4 – A2; see Fig. 24).

wavelet spectrum energy of spike-wave discharges fell. The results of searching for the source (focus) of epileptic activity and the temporal dynamics of hypersynchronous state formation are presented in Fig. 25. The lines connect pairs of channels between which synchronization occurred at an instant of time indicated by an appropriate arrow on the EEG. Evidently, synchronization starts a few seconds before the appearance of a spike-wave discharge on the EEG (diagram corresponding to synchronization at moment A in Fig. 25). As the spike-wave discharge evolves, the primarily synchronized part of the frontal cortex in the right hemisphere extends to the adjacent regions and the occipital region (time moment B). The epileptic focus (synchronization region prior to discharge) is localized in the frontal cortex, in good conformity with the known data [13, 183]. The development of the epileptic discharge is accompanied by the further extension of the synchronization region (time moments B and C). In this manner, the epileptic activity extends over the entire cerebral cortex. Evidently, the increasingly larger number of brain regions becomes involved in the synchronization process as the epileptic discharge develops; virtually all of them generate synchronized low-frequency oscillations by the middle of the spike-wave discharge (time moment D). By its end, the brain regions depart from the synchronous state (time moments E and F), which is reflected in the diagrams.

Thus, the time scale synchronization method based on the application of continuous wavelet analysis with the complex basis was successfully utilized for the description of space–time synchronization of brain electrical activity. Analysis of multichannel EEG recordings by this method allowed efficient localization of the source of epileptic activity and revealed its distribution patterns. These approaches may find application to the solution of other problems pertaining to the detection of links between different brain regions, searching for high-frequency brain activity related to cognitive abilities [186, 187], etc.

6. Conclusions

Wavelet analysis remains a somewhat exotic method in modern neurodynamics. As is known, any new method, even one providing a broader range of possibilities than traditional approaches, needs time to be converted into a convenient tool for routine application. It is especially true of the medico-biological sciences, where novel tools require a thorough checkup, adaptation, and verification to be accepted. In this context, it should be emphasized that wavelet analysis not only permits exposing new structural features of complicated neurophysiological signals, but also allows integration into combined algorithms for experimental data processing to enhance the efficacy of the existing methods widely applied in neurophysiological research. We believe that it is this evolutionary principle that will eventually turn wavelet analysis into a standard method for signal processing, not only in physics and mathematics, but also in biology and medicine. This implies not so much the replacement of conventional neurophysiological techniques by new ones, as the improvement of existing approaches to make wavelet analysis more popular among experimenting neurophysiologists.

Neurodynamics and neurophysiology make up an extensive area of the natural sciences. We were able to address only a very narrow set of problems in the present work. However, even this brief review demonstrates manifold possibilities and prospects for the application of wavelet analysis in neurophysiological research. The use of powerful tools of physicomathematical analysis of neural systems at the micro- and macrolevels of the central nervous system makes it possible to study at present the most complicated mechanisms underlying numerous brain functions. At the same time, interpretation of the results of such investigations in the context of neurophysiology is sometimes not a trivial task, due to the unprecedented complexity of the object under study (the nervous system of living organisms), on the one hand, and difficulties encountered in the interpretation of the results obtained by sophisticated neurophysiological methods. There is much truth in the remark made by A M Ivanitskii and A I Lebedev in their paper on the scientific legacy of M N Livanov that "the integration of mathematics and physiology gives the best result when the application of one mathematical transformation or another is underlain by a fruitful physiological idea" [188]. Indeed, a recipe for success of novel data processing technologies in the framework of interdisciplinary research in modern neurophysiology is the generation of new ideas and proper goal-setting.

There is little doubt that the number of neurodynamic studies using wavelets will continue to grow, because the solution to such challenging problems as the principles of information coding, presentation, and treatment in CNS requires not only the development of research and trial facilities (where considerable progress was made in the last few decades), but also new methods for decoding neural signals. The extreme complexity and many-sidedness of brain processes make it impossible to decipher neural signals only by the methods of statistical analysis. Adaptation of living organisms (including neural systems) to the environment is accompanied by changes in their dynamics, and the data of neurophysiological studies should be interpreted rather as resulting from nonstationary processes generated by dynamical systems with a very large number of degrees of freedom. Disregard of this fact reduces the possibility of

acquiring important information about neural systems, whereas understanding adaptation processes facilitates investigation into the underlying behavioral mechanisms. Wavelet analysis viewed as a sort of 'mathematical microscope' makes it possible under appropriate tuning to expose dynamic features unseen by the naked (or ill-equipped) eye; hence, the great (yet hidden) potential of this research tool. The present review was designed not only to describe some modifications of the analysis of experimental data (allowing us to address a number of problems pertaining to neural system dynamics), but also to instill the readers with our confidence in the promising prospects for the use of wavelets in neurodynamic applications. In the coming years, wavelet transform analysis can and must become an efficacious research tool for the improvement of research quality in the field of neurodynamics. To conclude, it should be emphasized that the newly proposed methods for the analysis of biological signals may find wide application in many areas of physics and technology.

Acknowledgments

The authors are deeply grateful to N A Brazhe and A R Brazhe for numerous discussions and the joint work on the analysis of intracellular dynamics, to G van Luijtelaar for many helpful considerations and the joint work covering the analysis of brain activity from recorded EEGs, and to O V Ivanov for advising on the discrete wavelet transform theory and the high-precision (64 discharges) calculations of coefficients of the Daubechies wavelet family that he provided for us.

The work was supported by RFBR (grants Nos 11-02-11000 and 12-02-00221), Federal Targeted Program 'Scientific and Scientific–Pedagogical Personnel of Innovative Russia' for 2009–2013, and Federal Targeted Program 'Research and Development in Priority Areas of the Russian Scientific and Technology Complex' for 2007–2013 (contract 11.519.11.2035).

References

1. Buzsáki G, Draguhn A *Science* **304** 1926 (2004)
2. Nekorkin V I *Usp. Fiz. Nauk* **178** 313 (2008) [*Phys. Usp.* **51** 295 (2008)]
3. Rabinovich M I, Muezzinoglu M K *Usp. Fiz. Nauk* **180** 371 (2010) [*Phys. Usp.* **53** 357 (2010)]
4. Tuckwell H C *Introduction to Theoretical Neurobiology* Vols 1, 2 (Cambridge: Cambridge Univ. Press, 1988)
5. da Silva F L *Electroencephalogr. Clin. Neurophysiol.* **79** 81 (1991)
6. Ivanitskii G R, Medvinskii A B, Tsyganov M A *Usp. Fiz. Nauk* **164** 1041 (1994) [*Phys. Usp.* **37** 961 (1994)]
7. Borisyuk G N et al. *Usp. Fiz. Nauk* **172** 1189 (2002) [*Phys. Usp.* **45** 1073 (2002)]
8. Freeman W J *J. Physiol. Paris* **94** 303 (2000)
9. Villacorta-Atienza J A, Velarde M G, Makarov V A *Biol. Cybern.* **103** 285 (2010)
10. Makarov V A, Villacorta-Atienza J A, in *Recurrent Neural Networks for Temporal Data Processing* (Ed. H Cardot) (Shanghai: InTech, 2011) p. 81
11. Nunez P L, Srinivasan R *Electric Fields of the Brain: The Neurophysics of EEG* (Oxford: Oxford Univ. Press, 1981)
12. Niedermeyer E, da Silva F L *Electroencephalography: Basic Principles, Clinical Applications, and Related Fields* (Philadelphia: Lippincott Williams & Wilkins, 2005)
13. Westmijse I et al. *Epilepsia* **50** 2538 (2009)
14. Ahissar E, Knutsen P M *Biol. Cybern.* **98** 449 (2008)
15. Makarov V A et al. *Comput. Intell. Neurosci.* **2010** 340541 (2010)
16. Grossmann A, Morlet J *SIAM J. Math. Anal.* **15** 723 (1984)
17. Daubechies I *Ten Lectures on Wavelets* (Philadelphia, Pa.: Society for Industrial and Applied Mathematics, 1992) [Translated into Russian (Moscow – Izhevsk: RKhD, 2001)]
18. Meyer Y *Wavelets: Algorithms and Applications* (Philadelphia: Society for Industrial and Applied Mathematics, 1993)
19. Meyer Y *Wavelets and Operators* (Cambridge: Cambridge Univ. Press, 1992)
20. Aldroubi A, Unser M (Eds) *Wavelets in Medicine and Biology* (Boca Raton: CRC Press, 1996)
21. Benedetto J J, Zayed A I (Eds) *Sampling, Wavelets, and Tomography* (Boston: Birkhäuser, 2004)
22. Letelier J C, Weber P P *J. Neurosci. Methods* **101** 93 (2000)
23. Hulata E, Segev R, Ben-Jacob E *J. Neurosci. Methods* **117** 1 (2002)
24. Quiroga R Q, Nadasdy Z, Ben-Shaul Y *Neural Comput.* **16** 1661 (2004)
25. Morlet J et al. *Geophysics* **47** 203 (1982)
26. Anfinogentov V G, Koronovskii A A, Hramov A E *Izv. Ross. Akad. Nauk Ser. Fiz.* **64** 2383 (2000)
27. Torrésani B *Analyse Continue par Ondelettes* (Paris: Savoirs Actuels, EDP Sciences 1995)
28. Addison P S *The Illustrated Wavelet Transform Handbook: Introduction Theory and Applications in Science, Engineering, Medicine and Finance* (Bristol: IOP Publ., 2002)
29. Koronovskii A A, Hramov A E *Nepreryvnyi Veivletnyi Analiz i Ego Prilozheniya* (Continuous Wavelet Analysis and Its Applications) (Moscow: Fizmatlit, 2003)
30. Kaiser G *A Friendly Guide to Wavelets* (Boston: Birkhäuser, 1994)
31. Mallat S *A Wavelet Tour of Signal Processing* (San Diego: Academic Press, 1999)
32. Astaf'eva N M *Usp. Fiz. Nauk* **166** 1145 (1996) [*Phys. Usp.* **39** 1085 (1996)]
33. Dremin I M, Ivanov O V, Nechitailo V A *Usp. Fiz. Nauk* **171** 465 (2001) [*Phys. Usp.* **44** 447 (2001)]
34. Van den Berg J C (Ed.) *Wavelets in Physics* (Cambridge: Cambridge Univ. Press, 2004)
35. Vetterli M, Kovačević J *Wavelets and Subband Coding* (Englewood Cliffs, N.J.: Prentice Hall, 1995)
36. Ali S T, Antoine J-P, Gazeau J-P *Coherent States, Wavelets and Their Generalizations* (New York: Springer, 2000)
37. Meyer Y, Coifman R *Wavelets: Caldéron-Zygmund and Multilinear Operators* (Cambridge: Cambridge Univ. Press, 1997)
38. Benedetto J J, Frazier M W (Eds) *Wavelets: Mathematics and Applications* (Boca Raton: CRC Press, 1994)
39. Koronovskii A A, Hramov A E *Nepreryvnyi Veivletnyi Analiz v Prilozheniyakh k Zadacham Nelineinoi Dinamiki* (Continuous Wavelet Analysis in Applications to the Problems of Non-Linear Dynamics) (Saratov: Kolledzh, 2002)
40. Gencay R, Selcuk F, Whitcher B *An Introduction to Wavelets and Other Filtering Methods in Finance and Economics* (San Diego, Calif.: Academic Press, 2002)
41. Strutz T *Bilddatenkompression. Grundlagen, Codierung, Wavelets, JPEG, MPEG, H.264* (Wiesbaden: Vieweg Braunschweig, 2002)
42. Walker J S *A Primer on Wavelets and Their Scientific Applications* (Boca Raton, Fla.: Chapman & Hall/CRC Press, 1999)
43. da Fontoura Costa L, Cesar R M (Jr.) *Shape Analysis and Classification: Theory and Practice* (Boca Raton, Fla.: CRC Press, 2001)
44. Jaffard S, Meyer Y, Ryan R D *Wavelets: Tools for Science & Technology* (Philadelphia: SIAM, 2001)
45. Wickerhauser M V *Adapted Wavelet Analysis from Theory to Software* (Wellesley, MA: A.K. Peters, 1994)
46. Postnikov E B, Lebedeva E A *Phys. Rev. E* **82** 057201 (2010)
47. Postnikov E B *Zh. Vychisl. Mat. Mat. Fiz.* **46** 77 (2006) [*Comput. Math. Math. Phys.* **46** 73 (2006)]
48. Hramov A E, Koronovskii A A *Chaos* **14** 603 (2004)
49. Torresani B, in *Self-similar Systems. Intern. Workshop, July 30 – August 7, 1998, Dubna, Russia* (Eds V B Priezzhev, V P Spiridonov) (Dubna: JINR, 1999) p. 9
50. Farge M *Annu. Rev. Fluid Mech.* **24** 395 (1992)
51. Meyers S D, Kelly B G, O'Brien J J *Mon. Weather Rev.* **121** 2858 (1993)
52. Pavlov A N *Izv. Vyssh. Uchebn. Zaved. Prikl. Nelin. Dinamika* **16** (6) 3 (2008)

53. Szu H, Telfer B, Garcia J *Neural Networks* **9** 695 (1996)
54. Koronovskii A A, Khramov A E *Fiz. Plazmy* **28** 722 (2002) [*Plasma Phys. Rep.* **28** 666 (2002)]
55. van Milligen B Ph et al. *Phys. Plasmas* **2** 3017 (1995)
56. Mouri H, Takaoka M *Phys. Rev. E* **65** 027302 (2002)
57. Bowman C, Newell A C *Rev. Mod. Phys.* **70** 289 (1998)
58. Argoul F et al. *Nature* **338** 51 (1989)
59. Quiroga R Q et al. *Phys. Rev. E* **65** 041903 (2002)
60. Foufoula-Georgiou E, Kumar P (Eds) *Wavelets in Geophysics* (San Diego: Academic Press, 1994)
61. Gusev V A, Koronovskii A A, Khramov A E *Pis'ma Zh. Tekh. Fiz.* **29** (18) 61 (2003) [*Tech. Phys. Lett.* **29** 775 (2003)]
62. Sitnikova E, Hramov A E, Koronovsky A A, van Luijtelaar G *J. Neurosci. Methods* **180** 304 (2009)
63. Koronovskii A A, Hramov A E, in *Nelineinye Volny — 2006* (Nonlinear Waves — 2006) (Exec. Eds A V Gaponov-Grekhov, V I Nekorkin) (Nizhny Novgorod: IPF RAN, 2007) p. 102
64. Hramov A E, Koronovskii A A *Physica D* **206** 252 (2005)
65. Hramov A E, Koronovskii A A, Levin Yu I *Zh. Eksp. Teor. Fiz.* **127** 886 (2005) [*JETP* **100** 784 (2005)]
66. Postnikov E B *Zh. Eksp. Teor. Fiz.* **132** 742 (2007) [*JETP* **105** 652 (2007)]
67. Sosnovtseva O V et al. *Phys. Rev. Lett.* **94** 218103 (2005)
68. Brazhe N A et al. *J. Biol. Phys.* **32** 191 (2006)
69. Brazhe A R et al., in *Handbook of Research on Systems Biology Applications in Medicine* (Ed. A Daskalaki) (Hershey, PA: Medical Information Science Reference, 2009) p. 653
70. Tychinskii V P *Usp. Fiz. Nauk* **177** 535 (2007) [*Phys. Usp.* **50** 513 (2007)]
71. Sosnovtseva O V et al. *Phys. Rev. E* **70** 031915 (2004)
72. Marsh D J et al. *Am. J. Physiol. Regul. Integr. Comp. Physiol.* **288** R1160 (2005)
73. Addison P S, Watson J N *Int. J. Wavelets Multiresolut. Inf. Process.* **02** 43 (2004)
74. Pavlov A N et al. *Brief. Bioinform.* **7** 375 (2006)
75. Arvidsson J *J. Comp. Neurol.* **211** 84 (1982)
76. Darian-Smith I, in *Somatosensory System* (Handbook of Sensory Physiology, Vol. 2, Ed. A Iggo) (Berlin: Springer-Verlag, 1973) p. 271
77. Hayashi H *Brain Res.* **183** 442 (1980)
78. Woolsey T A, Van der Loos H *Brain Res.* **17** 205 (1970)
79. Jacquin M F et al. *J. Neurophysiol.* **70** 1911 (1993)
80. Moreno A et al. *Neuroreport* **16** 1569 (2005)
81. Carvell G E, Simons D J *Somatosens. Mot. Res.* **12** 1 (1995)
82. Harvey M A, Bermejo R, Zeigler H P *Somatosens. Mot. Res.* **18** 211 (2001)
83. Garabedian C E et al. *J. Neurophysiol.* **90** 1379 (2003)
84. Pavlov A N *Proc. SPIE* **6436** 64360R (2007)
85. Welker W I *Behaviour* **22** 223 (1964)
86. Castellanos N P et al. *J. Neurophysiol.* **98** 2537 (2007)
87. Grinsted A, Moore J C, Jevrejeva S *Nonlin. Processes Geophys.* **11** 561 (2004)
88. Lewicki M S *Network Comput. Neural Syst.* **9** R53 (1998)
89. Schmidt E M *J. Neurosci. Methods* **12** 95 (1984)
90. Gray C M et al. *J. Neurosci. Methods* **63** 43 (1995)
91. Salganicoff M et al. *J. Neurosci. Methods* **25** 181 (1988)
92. Sarna M F et al. *J. Neurosci. Methods* **25** 189 (1988)
93. Zouridakis G, Tam D C *Comput. Biol. Med.* **27** 9 (1997)
94. Press W H et al. *Numerical Recipes in C: The Art of Scientific Computing* (Cambridge: Cambridge Univ. Press, 1992)
95. Pavlov A N et al. *Lecture Notes Comput. Sci.* **3561** 124 (2005)
96. Pavlov A et al. *Natural Comput.* **6** 269 (2007)
97. Haykin S *Neural Networks: A Comprehensive Foundation* (Upper Saddle River, NJ: Prentice Hall, 1999)
98. Kohonen T *Self-organization and Associative Memory* (Berlin: Springer-Verlag, 1989)
99. Hopfield J J, Tank D W *Biol. Cybern.* **52** 141 (1985)
100. Callan R *The Essence of Neural Networks* (Bristol: Prentice Hall Europe, 1999)
101. Kugarajah T, Zhang Q *IEEE Trans. Neural Networks* **6** 1552 (1995)
102. Cheng Y, Chen B, Shiau F *Proc. Natl. Sci. Counc. ROC A* **22** 783 (1998)
103. Chang P R, Weihui Fu, Minjun Yi *Eng. Intel. Syst. Elect. Eng. Commun.* **6** 217 (1998)
104. Cao L et al. *Physica D* **85** 225 (1995)
105. Abarbanel H D et al. *Usp. Fiz. Nauk* **166** 363 (1996) [*Phys. Usp.* **39** 337 (1996)]
106. Zanette D H, Mikhailov A S *Phys. Rev. E* **58** 872 (1998)
107. Strogatz S H *Nature* **410** 268 (2001)
108. Boccaletti S et al. *Phys. Rep.* **424** 175 (2006)
109. Destexhe A, Sejnowski T J *Thalamocortical Assemblies: How Ion Channels, Single Neurons, and Large-Scale Networks Organize Sleep Oscillations* (Oxford: Oxford Univ. Press, 2001)
110. Livanov M N *Prostranstvennaya Organizatsiya Protsessov Golovnogo Mozga* (Spatial Organization of Cerebral Processes) (Moscow: Nauka, 1972) [Translated into English (New York: Wiley, 1977)]
111. Osovets S M et al. *Usp. Fiz. Nauk* **141** 103 (1983) [*Sov. Phys. Usp.* **26** 801 (1983)]
112. Sviderskaya N E *Sinkhronnaya Elektricheskaya Aktivnost' Mozga i Psikhicheskie Protsessy* (Synchronous Electrical Activity of Brain and Psychic Processes) (Moscow: Nauka, 1987)
113. Sviderskaya N E *Prostranstvennaya Organizatsiya Elektroentsefalogrammy* (Spatial Organization of Encephalograms) (Moscow – Voronezh: Izd. VGMA, 2008)
114. Näätänen R *Attention and Brain Function* (Hillsdale, NJ: L. Erlbaum, 1992) [Translated into Russian (Moscow: Izd. MGU, 1998)]
115. Velichkovskii B M *Kognitivnaya Nauka: Osnovy Psikhologii Poznaniya* (Cognitive Science: Fundamentals of Cognitive Psychology) (Moscow: Akademiya, 2006)
116. Sviderskaya N E, Dashchinskaya T N, Taratynova G V *Zh. Vyssh. Nerv. Deyat.* **51** 393 (2001)
117. Wolpaw J R et al. *Clin. Neurophysiol.* **113** 767 (2002)
118. Guger C et al. *IEEE Trans. Neural Syst. Rehabil. Eng.* **11** 145 (2003)
119. Ivanitskii G A et al. *Voprosy Iskusstv. Intellekta* **1** (1) 93 (2008)
120. Kaplan A Y et al. *Int. J. Neurosci.* **115** 781 (2005)
121. Sitnikova E Yu, Koronovskii A A, Hramov A E *Izv. Vyssh. Uchebn. Zaved. Prikl. Nelin. Dinamika* **19** (6) 173 (2011)
122. Drinkenburg W H et al. *Physiol. Behav.* **54** 779 (1993)
123. Durka P J *Biomed. Eng.* **2** 1 (2003)
124. Freeman W J, Skarda C A *Brain Res.* **10** 145 (1985)
125. Jobert M et al. *J. Sleep Res.* **3** 223 (1994)
126. van Vugt M K, Sederberg P B, Kahana M J *J. Neurosci. Methods* **162** 49 (2007)
127. Slobounov S, Cao C, Sebastianelli W *Clin. Neurophysiol.* **120** 862 (2009)
128. van Luijtelaar G, Hramov A, Sitnikova E, Koronovskii A *Clin. Neurophysiol.* **122** 687 (2011)
129. Steriade M *Neuronal Substrates of Sleep and Epilepsy* (Cambridge: Cambridge Univ. Press, 2003)
130. Steriade M, McCormick D A, Sejnowski T J *Science* **262** 679 (1993)
131. Sitnikova E, van Luijtelaar G *Epilepsy Res.* **71** 159 (2006)
132. Kryukov A K et al. *Phys. Rev. E* **79** 046209 (2009)
133. Moeller F et al. *Epilepsia* **51** 2000 (2010)
134. van Luijtelaar G, Sitnikova E, Littjohann A *Clin. EEG Neurosci.* **42** 83 (2011)
135. Depaulis A, van Luijtelaar G, in *Models of Seizures and Epilepsy* (Eds A Pitkänen, P A Schwartzkroin, S L Moshé) (Burlington, MA: Elsevier/Academic Press, 2005) p. 233
136. Freeman W J *Mass Action in the Nervous System: Examination of the Neurophysiological Basis of Adaptive Behavior Through the EEG* (New York: Academic Press, 1975)
137. Steriade M, Deschenes M *Brain Res. Rev.* **8** 1 (1984)
138. Hramov A et al. *Chaos* **16** 043111 (2006)
139. Koronovskii A A et al. *Izv. Vyssh. Uchebn. Zaved. Prikl. Nelin. Dinamika* **15** (4) 34 (2007)
140. Casella G, Berger R L (Eds) *Statistical Inference* (Pacific Grove, CA: Duxbury, 2002)
141. Ovchinnikov A, Lüttjohann A, Hramov A, van Luijtelaar G *J. Neurosci. Methods* **194** 172 (2010)
142. Grubov V et al. *Izv. Vyssh. Uchebn. Zaved Prikl. Nelin. Dinamika* **19** (4) 91 (2011)
143. Leresche N et al. *Pflugers Arch.* **463** 201 (2012)
144. Kostopoulos G K *Clin. Neurophysiol.* **111** (Suppl. 2) S27 (2000)
145. Sitnikova E et al. *Brain Res.* **1436** 147 (2012)

146. Koronovskii A A et al. *Izv. Vyssh. Uchebn. Zaved. Prikl. Nelin. Dinamika* **19** (1) 86 (2011)
147. Brunelli R *Template Matching Techniques in Computer Vision: Theory and Practice* (Chichester, UK: Wiley, 2009)
148. Koronovskii A A et al. *Dokl. Ross. Akad. Nauk* **409** 274 (2006) [*Dokl. Biol. Sci.* **409** 275 (2006)]
149. Platt N, Spiegel E A, Tresser C *Phys. Rev. Lett.* **70** 279 (1993)
150. Heagy J F, Platt N, Hammel S M *Phys. Rev. E* **49** 1140 (1994)
151. Kim C-M *Phys. Rev. E* **56** 3697 (1997)
152. Boccaletti S, Valladares D L *Phys. Rev. E* **62** 7497 (2000)
153. Hramov A E, Koronovskii A A *Europhys. Lett.* **70** 169 (2005)
154. Moskalenko O I, Koronovskii A A, Hramov A E *Intermittent Behavior near the Boundary of Chaotic Synchronization: The Basic Properties and Regularities* (Saarbrucken: LAP LAMBERT Academic Publ., 2012)
155. Ovchinnikov A A et al. *Zh. Tekh. Fiz.* **81** (1) 3 (2011) [*Tech. Phys.* **56** 1 (2011)]
156. Tran Y et al. *Med. Biol. Eng. Comput.* **42** 627 (2004)
157. Urrestarazu E et al. *Epilepsia* **45** 1071 (2004)
158. Jung T P et al. *Clin. Neurophysiol.* **111** 1745 (2000)
159. James C J, Hesse C W *Physiol. Meas.* **26** R15 (2005)
160. Bell A J, Sejnowski T J *Neural Comput.* **7** 1129 (1995)
161. James C J, Gibson O J *IEEE Trans. Biomed. Eng.* **50** 1108 (2003)
162. Joyce C A, Gorodnitsky I F, Kutas M *Psychophysiology* **41** 313 (2004)
163. Flexer A et al. *Neural Networks* **18** 998 (2005)
164. Vigário R N *Electroencephalogr. Clin. Neurophysiol.* **103** 395 (1997)
165. Tong S et al. *J. Neurosci. Methods* **108** 11 (2001)
166. Jung T P et al. *Psychophysiology* **37** 163 (2000)
167. Schiff S J et al. *Electroencephalogr. Clin. Neurophysiol.* **91** 442 (1994)
168. Alegre M et al. *Exp. Brain Res.* **148** 17 (2003)
169. Goelz H, Jones R D, Bones P J *Clin. Electroencephalogr.* **31** 181 (2000)
170. Quian Quiroga R, Garcia H *Clin. Neurophysiol.* **114** 376 (2003)
171. Murata A *Hum. Factors* **47** 498 (2005)
172. Wan X et al. *Clin. Neurophysiol.* **117** 668 (2006); *Clin. Neurophysiol.* **117** 681 (2006)
173. Rong-Yi Y, Zhong C *Chinese Phys.* **14** 2176 (2005)
174. Castellanos N P, Makarov V A *J. Neurosci. Methods* **158** 300 (2006)
175. Amari S, Cichocki A, Yang H H *Adv. Neural Inform. Process. Syst.* **8** 757 (1996)
176. Lee T-W, Girolami M, Sejnowski T J *Neural Comput.* **11** 417 (1999)
177. Hyvärinen A, Pajunen P *Neural Networks* **12** 429 (1999)
178. Pivik R T et al. *Psychophysiology* **30** 547 (1993)
179. Friston K J *Trends Cogn. Sci.* **2** 373 (1998)
180. Donoho D L et al. *J. R. Statistical Soc. B* **57** 301 (1995)
181. Debnath L *Wavelet Transforms and Their Applications* (Boston: Birkhäuser, 2002)
182. Panayiotopoulos C P *Arch. Dis. Child.* **81** 351 (1999)
183. Gnezditskii V V *Obratnaya Zadacha EEG i Klinicheskaya Elektroentsefalografiya* (The Inverse Problem of EEG and Clinical Encephalography) (Taganrog: Izd. TRTU, 2000)
184. Zhuravlev M O et al. *Phys. Rev. E* **83** 027201 (2011)
185. Ovchinnikov A A et al., in *Nelineinaya Dinamika v Kognitivnykh Issledovaniyakh. Vseross. Konf., 2011 god, Nizhnii Novgorod. Tezisy Dokladov* (Nonlinear Dynamics in Cognitive Studies. All-Russian Conf., 2011, Nizhny Novgorod) (Nizhny Novgorod: Institut Prikladnoi Fiziki RAN, 2011) p. 140
186. Dumenko V N *Vysokochastotnye Komponenty EEG i Instrumental'noe Obuchenie* (High-Frequency EEG Components and Instrumental Training) (Moscow: Nauka, 2006)
187. Dumenko V N *Zh. Vyssh. Nerv. Deyat.* **57** 520 (2007)
188. Ivanitskii A M, Lebedev A N *Zh. Vyssh. Nerv. Deyat.* **57** 636 (2007)